NASA Contractor Report 4350

Control of Helicopter Rotorblade Aerodynamics

James A. Fabunmi

NASA Contractor Report 4350
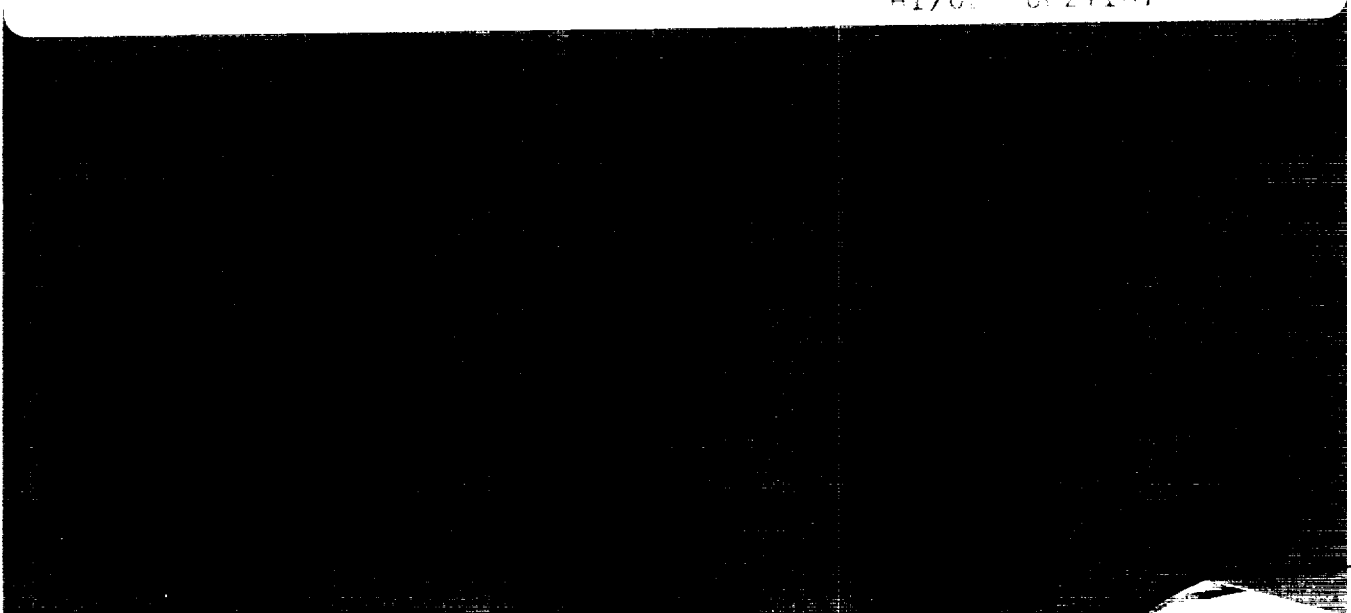
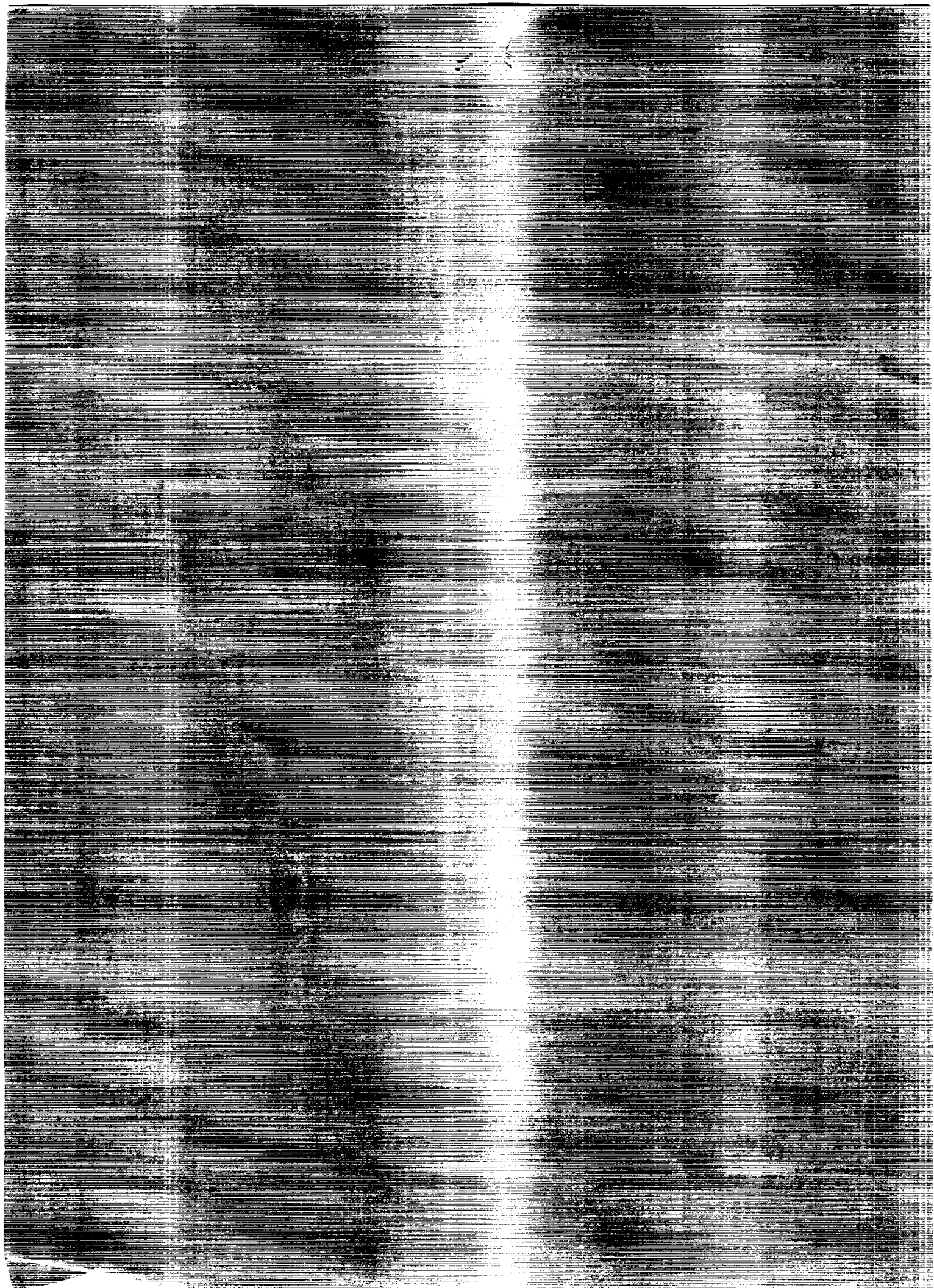# Control of Helicopter Rotorblade Aerodynamics

James A. Fabunmi
AEDAR Corporation
Landover, Maryland

Prepared for
Ames Research Center
under Contract NAS2-13095

Contents

List of Figures

Symbols and Abbreviations

$A(x), A_1, A_2$	cross sectional Areas
A/C	alternating Current
a_d	amplitude of oscillation of the driver
$(a_d)_{peak}$	peak amplitude of oscillation of the driver
APC	trademark of American Piezoceramics, Inc.
C_E	electrical capacitance
C_M	mechanical compliance
d, d_{31}, d_{33}	piezoelectric strain constants (see appendix)
$e, e(t)$	oscillatory displacement
F	force, mechanical resistance
F_{load}	loading force
F_{peak}	peak mechanical resistance
f	frequency
f_R	resonant frequency
$G(x, \chi, t)$	Green's function
G	gear
g	piezoelectric stress constant (see appendix)
H-2	trademark of Kaman Aerospace Corporation
i	electrical current; imaginary number, $i^2 = -1$
j	imaginary number, $j^2 = -1$
K, K1, K2	spring rates
k, k_{33}	piezoelectric coupling constants (see appendix)
L	length
m	effective mass of drive head
N	number of plates

N_{3t}	(thin plate) frequency constant
$(P_c)_{peak}$	peak power output, averaged over each cycle of oscillation of driver
$P_{electrical}$	electrical power
$P_{mechanical}$	mechanical power
PVDF	polyvinyledene fluoride
PZT,PZT-5H	trademarks of Clevite Corporation
q	electrical charge
R	drive head
R1,R2	rotary drive heads
S1,S2	stacks of piezoelectric plates
s^E, s^E_{33}	elastic compliance at constant electric field (see appendix)
s^D	elastic compliance at constant charge density (see appendix)
SBIR	Small Business Innovation Research
SH-2F	trademark of Kaman Aerospace Corporation
t	time, thickness
$T(x,t)$	internal axial force
u, u_{load}	velocities
U_r	translational velocity of chordwise rod
$(U_r)_{peak}$	peak translational velocity of chordwise rod
U.S.P.	United States Patent
V	voltage
$(V/t)_{max.}$	maximum field intensity
$(W_c)_{peak}$	peak mechanical work per cycle
$w(x,t)$	axial displacement
x	axial coordinate
Z_{load}	load impedance

$\alpha(x)$	$\equiv \partial \ln A(x)/\partial x$
χ	spatial coordinate
δx	displacement of actuator interface
ε	strain deformation
ε^S_{33}	relative dielectric constant of material when the faces are clamped (see appendix)
ε_0	dielectric constant of free space
Φ	electrical field intensity
$\Gamma(x,t)$	forcing function defined in Eq.(3.18)
λ	characteristic parameter
λ_k	k^{th} characteristic parameter
μ^2	$\equiv 1/(\rho.s^E_{33})$
ρ	mass density
$\sigma(x,t)$	internal axial stress
τ	time
ω	angular frequency
$\Psi(x)$	characteristic function
$\Psi_k(x)$	k^{th} characteristic function

Summary

The results of a feasibility study of a method of controlling the aerodynamics of helicopter rotorblades using stacks of piezoelectric ceramic plates are presented. A resonant mechanism is proposed for the amplification of the displacements produced by the stack. This motion is then converted into linear displacement for the actuation of the servoflap of the blades. A design which emulates the actuation of the servoflap on the Kaman SH-2F is used to demonstrate the fact that such a system can be designed to produce the necessary forces and velocities needed to control the aerodynamics of the rotorblades of such a helicopter. Estimates of the electrical power requirements are also presented. An SBIR Phase II research program is suggested, whereby a bench-top prototype of the device can be built and tested. A collaborative effort between AEDAR Corporation and Kaman Aerospace Corporation is anticipated for future effort on this project.

Chapter 1 - Introduction

This report has been prepared to present the objectives, approach, research performed and the results of the Phase I SBIR project aimed at establishing the feasibility of using stacks of piezoelectric ceramic actuators for controlling the deflection of servo-flaps on helicopter blades as a means of controlling the aerodynamics of the blade. The motivation for this work stems from the need to expand the flight envelopes of high performance helicopters. During high speed forward flight, the airfoil sees large variations of its upstream flow conditions within each revolution of the rotor. Existing control mechanisms are restricted to N-per-rev inputs from the non-rotating frame via some swashplate arrangement. The proposed concept will eliminate this restriction, and permit the input of any type of real time control needed to achieve optimal performance of the aerodynamic system.

The electromechanical properties of piezoelectric materials have been known for some time. These materials have been used extensively as sensors and low-energy actuators in low frequency applications and as high frequency ultrasonic exciters in a variety of applications. A survey of the state of the art and patents of applications which are somewhat related to the proposed concept is presented in Chapter 2. Tables of the properties of commercially available ceramics are also presented. The proposed application attempts to use stacks of piezoceramics in a high energy mode at relatively low frequencies. This is new. The analysis required to demonstrate the feasibility of these devices calls for a study of the design and kinematics of arrangements of piezoelectric plates stacked in such a way that they not only fit certain geometric constraints, but also deliver force and energy levels high enough for the intended applications. Chapter 3 presents the development of the analytical tools which were used in this study. The basic single element actuator are studied using a lumped parameter model. In order to deal effectively with the stacked multi-element actuator, a distributed parameter model is introduced, and the equations of motion which include the piezoelectric effects are developed. The numerical code which was developed for solving the equations for specific design configurations is also described.

As it turned out, not all the original concepts which were suggested in the SBIR proposal turned out to be feasible. Much of the analytical effort which was expended on those concepts did no more than establish that a different approach was needed if the requirements of large displacements typical of a servo-flap controlled helicopter rotorblade are to be met. It was realised that the coupling required in order to transfer significant

3

power from the stacks had to occur at very small displacements and in some oscillatory fashion. In other words, the actuation of the stacks had to be amplified by a resonant substructure which can then convert the energy stored in the oscillations into force and translation, sufficient to drive the linkage which ultimately deflects the servo-flap. In chapter 4, the principle of operation of the resonant actuator concept as well as the analysis of its load carrying capabilities are presented. Alternative designs are also examined with the objective of presenting options on how this concept can be implemented on a helicopter.

The study of the feasibility the proposed concept was based on the assessment of the ability of the device to generate control forces and displacements comparable to those of a known operating servoflap controlled rotorblade system. Measured data on the chordwise rod of the servo-flap controlled rotorblade of the Kaman SH-2F helicopter are used to estimate the required design loads for the proposed concept. Estimates of the electrical power requirements of a typical design are also presented. In the concluding remarks, it is stated that the use of piezoelectric ceramics for the control of helicopter rotorblade aerodynamics is feasible if the proposed resonant concept is implemented. A number of technological issues remain to be resolved before such a system can be ready for prototype testing. Issues such as the design of the system controllers and the control algorithms as well as the mechanical design of the linkage mechanisms which will permit bi-directional actuation are yet to be researched. AEDAR corporation hopes to compete for a Phase II SBIR support for the continuation of the research necessary to validate the operation of the proposed device. The Phase II effort will be directed at the construction of a bench-top model of the actuator which will permit the measurement of the force/ displacement characteristics of the device and will also support the development of a prototype design suitable for model-scale testing in a wind tunnel.

AEDAR corporation acknowledges the contribution of Kaman Aerospace Corporation in providing data on the measured control loads on the chordwise rod of the servo-flap control system on the SH-2F. Based on preliminary discussions with Dr. Andrew Lemnios of Kaman, it is anticipated that a collaborative effort between AEDAR corporation and Kaman Aerospace Corporation will be proposed for subsequent phases of this research. The SH-2F which is manufactured by Kaman is the only helicopter in the U.S. which employs a servo-flap to control the aerodynamics of the torsionally soft rotorblade. It is therefore expected that their experience in this area will be of substantial help in the development of an operational system which will employ the newly conceived technology.

Chapter 2 - State of the Art and Patents Survey

2.1 Applications of piezoelectric materials

Piezoelectricity or "pressure electricity" is a property of certain crystals such as quartz, Rochelle salt, tourmaline, ammonium hydrogen phosphate, and barium titanate. In response to applied pressure, electricity is developed by these materials. The reverse effect is also present - when an electric field is applied, the crystals change shape. More recently, the piezoelectric effect has also been discovered in ceramics such as lead zirconate-lead titanate ceramics and polymers such as PVDF (polyvinyledene fluoride). Piezoelectricity was first discovered by Pierre and Jacques Curie in the 19th century. Simple piezoelectric elements have found applications in such devices as:

- *Gasoline Engine Ignition* where the electrical sparks are generated by the periodic compression of a piezoelectric element by means of a cam-driven lever;
- *Underwater Sound Transducer* where sound pressure is coupled through water with stacks of piezoelectric crystal plates. The electrical signals generated are proportional to the acoustical pressures impinging on the device;
- *Microphones* which use piezoelectric diaphragms as active elements;
- *Phonograph Pickups* which utilize the bimorph arrangement of piezoelectric plates as transducers for converting the oscillatory motion of the stylus head into electrical signals which are subsequently amplified for audio reproduction of the recorded sounds;
- *Accelerometers* which use inertial masses mounted on piezoelectric elements to generate electrical signals in proportion to the acceleration of the masses;
- *Ultrasonic Transducers* which generate high frequency vibrations in applications such as machine part cleaning, ultrasonic physical therapy (massage) and various ultrasonic diagnostic devices used in Non-Destructive-Testing and in Medicine;
- *Strain Gages* which utilize strips of piezoelectric materials to sense deformations in solids by converting the mechanical strains to electrical signals directly without the need for external power supplies;
- *Structural Exciters* in experimental structural dynamics;
- *Structural Control Actuators* which use the reverse effect to impose local stresses on flexible structures in response to applied electrical signals which are programmed to introduce active damping into the structural system;
- *Distributed Pressure Sensors* on aero/hydrodynamic surfaces which use films of piezoelectric polymers as sensors of distributed pressures on

surfaces by converting the pressures directly into electricity which can then be processed to extract aero/hydrodynamic data;
- *Positioning Devices in Optics,* where piezoelectric elements are used to accomplish fine position adjustments of optical elements;
- *Rotary Machine Shaft Vibration Controllers* which is a relatively new application of piezoelectric bearing mounts which are energized in a manner such that cancellation forces are applied at the shaft mounts as a means of suppressing vibrations.

The preceding list of applications is by no means exhaustive. It merely serves to illustrate the versatility of these materials. It can be noted that most of the applications of piezoelectric materials involve small power and small deflection devices. The application to which this research is directed is seeking to break new grounds in terms of the power consumption and the displacements required of the actuator. It is therefore important at every stage of the research to be mindful of the physical constraints which must be circumvented in order to make this technology a reality. It must not be precluded that new material technologies might be called for, before one can be fully confident that the new concepts can be operated reliably under the extreme dynamic and environmental conditions to which helicopter rotorblades are subjected. The following section surveys a selection of commercially available piezoelectric ceramics and presents some pertinent data as published by the manufacturers of these devices. This data is presented here strictly for the sake of completeness of this report and does not imply any endorsements by the AEDAR Corporation of any of the products, vendors or manufacturers. AEDAR Corporation is not responsible for the accuracy of any of the information presented herein.

2.2 Properties of Some Commercially Available Ceramics

The most readily available piezoelectric ceramics are made of lead-zirconate-titanate and lead metaniobate compositions[1,2]. Some ceramics are also available which are made of barium titanate or modifications thereof. In addition to ceramics, there are polymers such as polyvinyledene fluoride (PVDF) which exhibit piezoelectric behavior[3]. The most popular applications for piezoelectric ceramics and polymers are those where the permissible strains and deflections are very small - of the order of microinches. In applications where the requirements are such that more deflection is required, the load-carrying capabilities have to be minimized. The primary coefficients which are used to assess the electromechanical transformation of energy are: coupling constant k, strain constant d and stress constant g. Coupling is an expression for the ability of a piezoelectric material to exchange electrical energy for mechanical energy or vice versa. Coupling squared is equal to the transformed energy divided by the total input energy. The d

constants express the ratio of strain developed along or around a specified axis, to the field applied parallel to a specified axis, when all external stresses are constant. The g constants express the ratio of field developed along a specified axis to the stress applied along or around a specified axis when all other external stresses are constant; it is also the ratio of strain developed along or around a specified axis to the electric charge per unit area of electrode applied to electrodes which are perpendicular to a specified axis. There are also the elastic constants s^D and s^E which specify the strain to stress ratios at open and short circuits respectively.

Piezoelectric materials are anisotropic - their electrical, mechanical, and electromechanical properties differ for electrical or mechanical excitation along different directions. The reference axes for the data on these coefficients are usually specified as numerical subscripts 1 through 6 (1,2,3 refer to linear actions along the axes, 4,5,6 refer to rotational actions about axes 1,2,3 respectively). Before the ceramics can exhibit piezoelectric properties, they have to be polarized by a strong electric field. The direction of the poling field is identified as the 3 direction. In the plane perpendicular to the 3 axis, the ceramics are nondirectional. Hence the 1 and 2 axes may be arbitrarily assigned, provided they are perpendicular to each other.

For the proposed application, it is desirable for the piezoelectric material to have the maximum possible coupling and strain constants. The highest rated piezoelectric ceramics are compositions containing lead zirconate and lead titanate. They are available under various trade names e.g. PZT (Clevite Corporation), APC (American Piezoceramics, Inc.) etc. Typical values of the piezoelectric constants for these ceramics are presented in the Appendix (Tables I through IV of the appendix were obtained from Ref. 1).

2.3 Review of Recent Patents on Large-Displacement Piezoelectric Actuators

Under the general class of devices which can be referred to as piezoelectric motors, several United States Patents (U.S.P.) have been granted within the past two to three years. A common thread through all these devices is the utilization of incremental actions at high frequencies to achieve large displacements or rotations. This section will present a brief survey of the basic principles underlying these patents. Detail description of the devices are availble in the referenced patent documents. The goal of this review is to ascertain whether or not any of the newly proposed concepts have been applied somewhere else. It is ofcourse unavoidable that new ideas can be learned from the various

7

approaches that have been adopted by other inventors.

In U.S.P. # 4,709,183 (Nov. 24, 1987), Jurgen Lange (West Germany) described a linear motor consisting of a framelike stator and a multi-element sliding rotor. The rotor assembly consists of piezoelectric elements which are fed with electric signals such that by combining the longitudinal expansion and contraction of a connecting element with the transverse expansion and contraction of two traction elements, a creeping effect is achieved. No data was presented about the force/speed characteristics of the motor. The demands of close tolerances along with the dimensional constraints on the elements of this device will not make it suitable for the control of servoflaps in the type of evironment that is of interest here. U.S.P. # 4,714,855 (Dec. 22, 1987) is an invention by Toshitaka Fujimoto (Japan) wherein the piezoelectric motor consists of a disk rotor and a stator assembly in which an arrangement of piezoelectric elements are used to control the sequential clamp-release-rotate-clamp cycle of the rotor. This is roughly a rotary implementation of the previous device by Jurgen Lange. There was no data presented on the force/speed characteristics, however the same limitations observed earlier are expected to hold for this device also.

On April 5, 1988, U.S.P. # 4,736,129 was granted to Akira Endo and Nobutoshi Sasaki (Japan) for an Ultrasonic Motor. The rotor and stator can be either linear or rotary and the contact between them is via a material which has to have carefully selected hardness characteristics. The reason for this is that the motion of the rotor relative to the stator is accomplished by means of travelling surface elliptical waves which are imposed on the piezoelectric stator. The mechanical coupling between the stator and the rotor is extremely sensitive to the hardness characteristics of the interface. If the interface is too soft, the travelling waves will be dampened; if it is too hard, elastic wave vibrations and frictional forces cause noise and heat without achieving much mechanical coupling. The performance data provided showed that both the speed and force (or torque) generated are maximum at certain values of the hardness of the contact material. A difficulty which was also acknowledged in the patent description is that with time, the contact material properties change due to heating effects. This makes the operation of this motor in rugged environments rather unstable. Another patent was granted to Toshikata Fujimoto on April 5, 1988 (U.S.P. # 4,736,131) for a linear motor driving device. The rotor includes a pair of actuators each having piezoelectric elements and kinematic displacement amplifiers arranged in such a way that the linear rotor can propel itself along the tracks in the stator by means of programmed energization of the actuators similar to the gait of a four legged animal. No performance data was presented. An apparent limitation of this device is the load carrying capabilities. A pair of shaft mounted circumferentially contacting disks with one of the disks having an arrangement of piezoelectric elements, is the idea behind U.S.P. # 4,755,705 granted to Mark J. Holum (U.S.) on July 5, 1988. The reactive

forces generated at the disk contact points by programmed energization of the radially distributed piezoelectric elements causes the disks to rotate in opposite directions. The torque/speed characteristics of the device was not presented, however it is clear that continuous contact has to be maintained between the disks. In a vibratory environment like the helicopter rotorblade, this idea does not hold much promise.

The travelling wave concept was again used in U.S.P. 4,786,836 by Akira Tokushima (November 22, 1988), except that a stronger coupling mechanism is employed to overcome the difficulties associated with the Endo et al. device. The motor can be configured to be either linear or rotary. Travelling wave vibrations are induced by piezoelectric elements in the stator. These waves are coupled to the rotor via an arrangement of sliders. Speeds of up to 350 rpm in the rotary mode and 0.5 m/s at peak to peak voltages of 100 volts were reported. Torque data was presented in relative units, so that it is not clear what levels of power can be delivered by this device. Again, in a severe vibratory environment, this principle of operation may not be adequate. The applications for which most of these devices have been envisaged are clearly those in which narrow tolerances can be maitained and enviromental vibration is minimal, e.g. optical component positioning, micromotors in medical systems, etc. In seeking to employ piezoelectrics in an environment where severe vibrations are the rule rather than the exception, it is desirable to have a system which is structurally compatible with the major load bearing members. In the case of the helicopter rotor blade, the stacks of piezoceramics should be integrated into the design of the blades somehow. Weight considerations also support this approach. If a separate motor module has to be employed, then one must show that its additional weight penalties are not excessive, otherwise the whole purpose of using piezoelectrics will be defeated, and one may as well resort to compact electric motors.

Chapter 3 - Studies of Actuator Design and Kinematics

3.1 Analytical Framework for Actuator Studies

The methods employed in this feasibility study are combinations of first-principle analysis, empirical data and some comaparisons with measured data on an existing helicopter. The goal of the analysis was to obtain estimates of the limiting performance parameters of various design concepts, such that some judgement can be made regarding the feasibility of the concepts. A condiderable amount of simplifying assumptions are inevitable in such an excercise since there is no experimental data to provide the parameters of known real world effects such as damping, internal losses, friction etc. At the interface between an actuator and the rest of the world, it is of interest to know performance characteristics such as force (or torque), displacement (or rotation), speed (or angular velocity). From the applications standpoint, certain values of these performance characteristics are required to establish feasibility. In many instances, immediate gross calculations based on the physical properties of the materials and the geometrical constraints on the design, can be used to show that a given design is clearly not feasible. A lot of such analyses were performed during the course of this research effort. The analytical models and results which will be described in subsequent sections in this chapter, are those which required detail calculations before any conclusions could be made regarding feasibility.

In the original proposal for this project, several concepts were sketched out for the accomplishment of controlled deflections of rotorblade mechanizations. The concepts which were based on the bimorph (or multimurph) and shear modes of deflection of the piezoelectric elements were dismissed based on preliminary data on commercially available ceramics and polymers. The bimorphs and multimorphs are incapable of delivering sufficient force, while the shear modes could not generate sufficient motions. This is not to say that new materials will not be invented that will change this assessment. The focus of this research is in seeking concepts that can be further developed into operational devices based on available technology. The concepts that were pursued further are based on the thickness expansion/contraction mode. First, the single element actuator was examined, whereby a single layer of piezoelectric ceramic is considered. The classical lumped parameter analytical model was used. Then the multilayered actuator was studied. Here, because of the possiblity that large and variable geometries can be involved, a more elaborate analysis based on a distributed parameter model was used. The

piezoelectric effect was included in the constitutive relation which describes the stress/strain relationships for the material.

3.2 Single Element Thickness Expansion/Contraction Actuator

The single element thickness expansion/contraction actuator shown in Fig. 3.1 represents the simplest configuration of a piezoelectric actuator. An electrical potential applied accross the electrodes causes a strain deformation which is proportional to the applied electrical field when all external stresses are kept constant (e.g. no restraint in any direction);

$$\varepsilon = d_{33}.(V/t) \tag{3.1}$$

where ε is the strain deformation, d_{33} is the piezoelectric strain constant when the direction of the applied field is parallel to the direction of the strain deformation, V is the applied voltage and t is the spacing between the electrodes (thickness of the element). This same piezoelectric constant relates the charge per unit area of electrode flowing between connected short circuited electrodes, to the stress applied along the axis perpendicular to the faces of the electrodes;

$$(q/A) = d_{33}.\tau \tag{3.2}$$

where q is the electrical charge, A is the surface area, and τ is the external stress. For the specific case of the thickness expansion/contraction actuator, $\varepsilon = \delta x/t$, and $\tau = F/A$, where δx is the displacement of the actuator interface, F is the external force applied at actuator interface, Eq. 3.1 and 3.2 can be rewritten as;

$$\delta x = d_{33}.V \tag{3.1a}$$

and,

$$q = d_{33}.F \tag{3.2a}$$

For electromechanical modelling purposes, it is preferable to deal in velocities and electrical currents (these being the primary power variables), rather than displacements and charges. For harmonic time variations, velocity $u = (j\omega)\delta x$ and electrical current $i = (j\omega)q$, where j is imaginary $(j^2 = -1)$ and ω is the frequency. The eletromechanical model for the single element piezoelectric actuator is shown in Fig. 3.2.

The lumped parameter model of the piezoelectric actuator is depicted as a transformer which converts electrical power variables to mechanical power variables according to the Eq. (3.1) and (3.2). The impedance analogy is utilized on the mechanical side of the transformer. At frequencies below the resonance of the piezoelectric plate, the mass and reactance elements are neglected. Also, partly because of the difficulty in modelling their values, and partly because of the need to keep the model simple, dissipative elements on both sides of the transformer are also neglected. The capacitance on the electrical side C_E is measured at low frequencies with the mechanical terminals open-circuited (u = 0; i.e. the faces of the element are mechanically restrained). The mechanical compliance C_M is measured with the electrical terminals short-circuited (V = 0). The transformer ratio $1 : C_E/d_{33}$ is verified as follows: at open mechanical circuit, application of a current i to the primary will produce a voltage accross the condenser C_E of $i/(j\omega C_E)$. This in turn produces an open-circuit force $F = (i/(j\omega C_E)).(C_E/d_{33}) = i/(j\omega d_{33}) = q/d_{33}$ as required by Eq. (3.2a). Conversely, at open electrical circuit, a velocity u at the secondary of the transformer produces a current through the condenser C_E equal to uC_E/d_{33} which in turn generates an open-circuit voltage of $V = (uC_E/d_{33})/(j\omega C_E) = \delta x/d_{33}$ consistent with Eq. (3.1a).

In lieu of measured data, the following expessions can be used to estimate the circuit parameters C_E and C_M;

$$C_E = (\epsilon^S_{33}/\epsilon_0).\epsilon_0.A/t \tag{3.3}$$

$$C_M = (t/A).s^E_{33} \tag{3.4}$$

where ϵ^S_{33} is the relative dielectric constant of the material when the faces are clamped, $\epsilon_0 = 8.85 \times 10^{-12}$ farads/meter is the dielectric constant of free space and s^E_{33} is the elastic compliance at constant electric field when both strain and stress are occuring along the 3 axis. The force F_{load} and velocity u_{load} at the load interface are:

$$F_{load} = (V.C_E/d_{33}).Z_{load}/(Z_{load} + 1/(j\omega C_M)) \tag{3.5}$$

$$u_{load} = F_{load}/Z_{load} \tag{3.6}$$

13

where Z_{load} is the load impedance.

3.3 Multiple Element Thickness Expansion/Contraction Actuator

The single element actuator model of the preceding section is very useful for gaining insight into the capabilities of piezoelectric transducers. By studying the preceding equations, it becomes evident how to go about designing the geometry and kinematics of actuators for specific purposes. Ironically, the physical data on piezoelectric materials, when substituted in to these equations, tends to indicate that these devices are feasible only at very low power and displacement levels. For example, the piezoelectric constant d_{33} is of the order of 10^{-10} meters/volt. The key to the design of piezo-actuators for larger displacements and larger power delivery, is to note the following facts; the piezoelectric constant d_{33} relates the strain developed to the *field intensity* (voltage per unit length), so that the actual limitation on the strain that can be developed is really the field intensity at which depoling occurs. The field intensity can be increased not only by increasing the available voltage supply, but also by decreasing the separation between the electrodes (i.e. reducing the thickness). Also, the force developed is related to the current flowing between the electrodes. This means that a large capacitance is needed between the electrodes. This can be achieved by increasing the surface area of the electrode faces. Both requirements of reducing the thickness and including the electrode area suggest the utilization of several thin plates stacked in such a way that when the same voltage is applied to every other electrode, with the interlacing electrodes grounded, the effect is to apply the same field intensity to all the plates and the total surface area of the electrodes is summed from all the areas of all the surfaces between the plates. By adopting this approach, any length of the stack can be assembled to provide the net displacement and the current flow needed for any application for which the geometric design permits such an assembly.

The schematic in Fig. 3.3 is used to study the dynamics of a multi-element thickness expansion/contraction actuator. A stack of N thin plates, thickness t (yielding an overall thickness of L = N.t) and having variable cross-sectional area A(x) is fed with a voltage V in such a way that alternating faces of the plates are simultaneously energized while the other sides are collectively grounded. The poling of the plates must ensure that the piezoelectric deformations are properly alligned. This arrangement assures that the same field intensity is impressed on all the plates, and hence the entire stack can be considered as being under the field intensity $\Phi = V/t$. The assembly is now considered as a distributed parameter "rod" undergoing longitudinal deformations under

14

elastic and piezoelectric internal stresses, subject to the boundary conditions of the applied loading forces, as well as the rigid support at the fixed end.

The standard approach for setting up the equations for this system is to consider the equilibrium of an infinitessimal element of the "rod" (see Fig. 3.4). It deserves to be noted that the centrifugal effects of blade rotation is not yet being considered because the initial designs anticipated have the plates stacked along the chord of the blade. If it becomes necessary to stack the plates radially, then it must be considered that the centrifugal forces will contribute to the equilibrium that is about to be examined.

$T(x,t)$ is the internal axial force in the stack (in the appropriate context, the letter t is used to denote the time variable, in contrast to earlier usage for thickness), $A(x)$ is the variable cross-sectional area, $w(x,t)$ is the axial displacement of the stack at coordinate x at the instant t; $\sigma(x,t)$ is the internal axial stress perpendicular to the plane of the cross-section; $T(x,t) = \sigma(x,t).A(x)$; ρ is the mass density of the material of the plates (noting that the electrode material at the surfaces may affect the value of this density for a sufficiently large number of plates per unit length); ρ is assumed to be constant. The equation for axial equilibrium of this element is:

$$\partial T(x,t)/\partial x - \rho.A(x).\partial^2 w(x,t)/\partial t^2 = 0 \tag{3.7}$$

The constitutive relationship between stress and strain taking the piezoelectric effect into account is:

$$\partial w(x,t)/\partial x = s^E_{33}.\sigma(x,t) + d_{33}.\Phi(t) \tag{3.8}$$

Hence the internal axial force and its spatial derivative are given by:

$$T(x,t) = \{ \partial w(x,t)/\partial x - d_{33}.\Phi(t) \}.A(x)/s^E_{33} \tag{3.9}$$

and,

$$\partial T(x,t)/\partial x = [\{ \partial w(x,t)/\partial x - d_{33}.\Phi(t) \}.\partial A(x)/\partial x + A(x).\partial^2 w(x,t)/\partial x^2]/s^E_{33} \tag{3.10}$$

The differential equation for the axial displacements of the stack is obtained upon substitution of Eq. (3.10) into Eq. (3.7) as:

$$\partial^2 w(x,t)/\partial t^2 - \mu^2.\partial^2 w(x,t)/\partial x^2 - \mu^2.\alpha(x).\partial w(x,t)/\partial x = -\mu^2.\alpha(x).d_{33}.\Phi(t) \tag{3.11}$$

where $\mu^2 \equiv 1/(\rho.s^E_{33})$ is the square of a velocity parameter related to the propagation of stress waves along the axis of the stack; and $\alpha(x) \equiv \partial \ln A(x)/\partial x$; the boundary conditions are:

$$w(0,t) = 0 \tag{3.12}$$

at the fixed end of the stack and,

$$\partial w(L,t)/\partial x = d_{33}.\Phi(t) - s^E_{33}.F_{load}(t)/A(L) \tag{3.13}$$

at the driving end of the stack. For the expediency of solving the differential equa-

15

tion using Green's Function techniques, a dependent variable substitution is sought which will transform the boundary conditions to homogenous ones. Let,

$$v(x,t) = w(x,t) - x.[\; d_{33}.\Phi(t) - s^E_{33}.F_{load}(t)/A(L)\;] \tag{3.14}$$

The differential equation governing $v(x,t)$ is,

$$\partial^2 v(x,t)/\partial t^2 - \mu^2.\partial^2 v(x,t)/\partial x^2 - \mu^2.\alpha(x).\partial v(x,t)/\partial x = -\mu^2.\alpha(x).d_{33}.\Phi(t) - x.[\; d_{33}.d^2\Phi(t)/dt^2 - (s^E_{33}/A(L)).d^2 F_{load}(t)/dt^2\;] + \mu^2.\alpha(x).[\; d_{33}.\Phi(t) - s^E_{33}.F_{load}(t)/A(L)\;] \tag{3.15}$$

subject to the homogenous boundary conditions: $v(0,t) = 0$, and $\partial w(L,t)/\partial x = 0$. The procedure used in solving for the response of this system is as follows. Define an eigenvalue problem,

$$\mu^2.d^2\Psi(x)/dx^2 + \mu^2.\alpha(x).d\Psi(x)/dx = \lambda^2\Psi(x) \tag{3.16}$$

subject to the boundary conditions: $\Psi(0) = 0$ and $d\Psi(L)/dx = 0$ as well as the normalizing condition: $\int_0^L \Psi(x)^2 dx = 1$. Note that if the cross-sectional area is uniform, $\alpha(x) = 0$ and these characteristic functions are simple trigonometric functions. However, for the general design case, a numerical algorithm was used for computing these functions. Also, because the application is at low frequencies (below the first resonance of the system), only a few lower order functions and parameters are needed. The Green's Function, $G(x,\chi,t)$ for this system is given by[4,5]:

$$G(x,\chi,t) = \Sigma(1/i\lambda_k)\Psi_k(x)\Psi_k(\chi).\sin(i\lambda_k t) \tag{3.17}$$

where i is the imaginary unit (i.e. $i^2 = -1$). By considering the right hand side of Eq. (3.15) as a forcing function:

$$\Gamma(x,t) \equiv -\mu^2.\alpha(x).d_{33}.\Phi(t) - x.[\; d_{33}.d^2\Phi(t)/dt^2 - (s^E_{33}/A(L)).d^2 F_{load}(t)/dt^2\;] + \mu^2.\alpha(x).[\; d_{33}.\Phi(t) - s^E_{33}.F_{load}(t)/A(L)\;] \tag{3.18}$$

The solution of Eq. (3.15) is obtained as:

$$v(x,t) = \int_0^t\!\int_0^x G(x,\chi,t-\tau)\Gamma(\chi,\tau)d\chi d\tau \tag{3.19}$$

The displacement response at the driving end of the stack is:

$$w(L,t) = \int_0^t\!\int_0^L G(x,\chi,t-\tau)\Gamma(\chi,\tau)d\chi d\tau + L.[\; d_{33}.\Phi(t) - s^E_{33}.F_{load}(t)/A(L)\;] \tag{3.20}$$

In the preceding derivations, the external load has been assumed to be an explicit function of time. In reality this load is related to the displacement at the driving point by the dynamic characteristics of the load itself. Invariably, this information is available in terms of an impedance of the load which relates the force applied to the velocity at the driving point. In such a case, there are two alternative approaches for calculating the response of the system. The first is to consider the load itself as a dynamic modification to the driving system, in which case, techniques such as those used in Ref. 6 can be used, or the dynamics of the load can be included in the equations used for obtaining the Green's function. For the scope of this feasibility research, the above equations are sufficient

16

for investigating whether or not the proposed designs can generate the force and displacements needed for the intended application, within the geometric and dynamic constraints of a helicopter rotorblade design. For this purpose, a steady value for the load is assumed which is least greater than the maximum time varying load anticipated during the operation of the device.

3.4 Conceptual Designs for Helicopter Rotor Applications

This section of the report presents the results of the exploratory analysis of the concepts which were proposed in the Phase I SBIR proposal. The basic approach was to analyze each concept for the purpose of determining the deflections that are possible, as well as the loads which can be developed. In most of the cases examined, the lack of measured wind tunnel data kept open the question as to whether the feasible deflections are sufficient to provide adequate control of the rotorblade aerodynamics. One concept however deserved detail treatment, from the standpoint that the arrangement of the piezoelectric actuator could be such that forces and deflections in excess of those that are needed in a real servoflap controlled helicopter, can be demonstrated. This idea - the resonant concept - is described in furthre details in Chapter 4.

The Direct Bimorph Concept: The schematic in Fig. 3.5 shows an arrangement whereby the aft section of the airfoil in a segment of the rotor blade is composed of layers of thin piezoelectric plates. The plates are energized with a distribution of electrical voltage such that the variation of the strains in the layers results in a flexing action of the airfoil. The field intensity at the outer layer is maximum and decreases nearly linearly towards the middle layers, reversing sign at the elastic axis of the section. The effect of this is to impress maximum extensional strains at one outer layer, while impressing maximum contractional strains at the outer layer of the other side.

The pertinent piezoelectric constant for this arrangement is d_{31}, since the direction of field application and that of the elastic strains are perpendicular. The material with the highest d_{31} is PZT-5H at a value of -274×10^{-12} meters/volt. At a maximum field strength of 10^5 volts/meter and a blade thickness/chord ratio of 0.16, the achievable angular deflection of the blade chordline is of the order of 2 $\times 10^{-4}$ radians. This does not appear to be appreciable enough to affect the aerodynamics of the blade. This finding also impacts on the feasibility of the bimorph hinged flap concept (see Fig. 3.6) which was also suggested in the original proposal. A piece of hindsight with regards to the bimorph hinged flap concept is the fact that the resonant concept which was later found to work for the thickness expansion/contraction modes (see chapter 4), can also be explored using the bimorph hinged flap

17

configuration. However, this research was not performed due to the limited scope of the funded effort.

Transverse Shear Hinged Flap Concept: In the schematic of Fig. 3.7, a stack of piezoelectric actuators are excited in the transverse shear mode. The deflection at the end of the stack is used to drive the rotation of the hinged flap. The shear deflections of the elements of the stack are governed by the piezoelectric constant d_{15}, which for PZT-5H is 741×10^{-12} meters/volt. The shear deflection of each element, at a field strength of 10^5 volts/meter is therefore of the order of $.741 \times 10^{-4}$ radians. In order for this to amount to anything at the tip of the stack, the dimensions of the stack will be unfeasible for a device that must fit the geometric boundaries of a helicopter rotorblade.

Thickness Expansion/Contraction Hinged Flap Concept: The direct coupling of the motions at the tip of a stack of piezoelectric plates which are excited in the thickness expansion/contraction (d_{33}) mode was the original idea proposed in the SBIR Phase I proposal (as shown in Fig. 3.8). Using a value of $d_{33} = 593 \times 10^{-12}$ meters/volt, and an electrical field intensity of 10^5 volts/meter, unloaded strains of only about $.593 \times 10^{-4}$ are achievable. This means that for every meter of the stack, the motions at the tip is only 0.0593 millimeters. This is obviously too small for any practical design.

The coupling of the stack to the drive head of the flap hinge can be amplified dynamically via a resonant substructure, one end of which is driven by the stack, the other end of which is connected to the flap hinge drive. This idea actually evolved during the review of existing patents on large-displacement piezoelectric actuators. It was quite apparent that no one in their right minds attempted to utilize the direct piezoelectric action to achieve large motions. Rather, everyone of the published shemes utilized some form dynamic amplification in the form of rapid incremental motions. The resonant concept for servoflap actuation is described more fully in the next chapter.

18

Chapter 4 - The Resonant Concept for Servoflap Actuation

4.1 Principle of operation of device

The schematic in Fig. 4.1 illustrates the arrangement which is suggested for the actuation of the servoflap on a helicopter rotor blade. S1 and S2 are stacks of piezoelectric plates (the shapes of these plates can be such that they fit into the design of the blade structure in a suitable manner. The design parameters of these plates are N, the number of plates, t, the thickness of each plate, and A the area of the plate surface (which can vary in a manner suitable to the geometry of the blade). K1 and K2 are sections of a lightly damped dual-cantilevered beam which act as elastic springs. R1 and R2 are the drive-heads which rotate the servoflaps about the hinge axis. The schematic is not shown to scale and the final design will consider specific constraints necessary to make the assembly fit a given rotor blade system.

In Fig. 4.2, a concept for the rotation of the servoflap about the hinge axis is shown. This is basically a ratchet mechanism which converts the linear oscillatory motions of the drive head R into the rotary motion of the gear G. The shape of the gear teeth is designed in such a way that little resistance is presented to the relative motions of the gear and the drive head during the return stroke. The drive stroke of one side is the return stroke of the other. In such a way, the motion of the drive head in both directions is used to advance the rotation of the gear. The drive head/gear combination for the other arm of the resonant system is arranged in such a way that they cause rotation of the servoflap in the opposite direction. When both drives are engaged with the gears, the piezoelectric drivers are turned off, and the flap is held in its undeflected state. When deflection is desired in a given direction, the appropriate drive is engaged and the piezo-drivers are turned on. To reverse the direction of flap rotation, the other driver is engaged while the former is disengaged. The programming of the control signals for achieving these actions are part of the design of the controller for the system.

The principle of operation of this drive system is that when the frequency of oscillations of the piezoelectric stack reaches a certain value, the motion of the drive heads will be amplified by the resonance of the spring-mass system comprising of the cantilever beam K1 or K2 along with the mass of the drive head itself. The resistance to the motion of the drive heads which is constituted by the forces required to rotate the gear for deflecting the servoflaps, plays the role of a damper for the resonant oscillations. For the oscillations to be sustained, the

19

power flow from the piezoelectric drivers must exceed the power expended on the motion of the flaps.

4.2 Feasibility Study

Simplified Analysis: For purposes of establishing the conceptual feasibility of the proposed device, an analytical model consisting of a base-driven spring-mass system is considered. In order for the system to operate, the electrical input into the piezoelectric stack must generate an oscillatory displacement determined by the maximum force which must be overcome by the ratchet head. The schematic of Fig. 4.3 illustrates a base-driven spring-mass model which is used to study the operation of the proposed device. The base driver consists of a stack of piezoelectric elements operating in the thickness expansion mode. This mode is expected to provide the maximum electromechanical energy conversion and coupling. This stack operates as a constant displacement generator which inputs an oscillatory displacement:

$$e(t) = e \cos \omega t \tag{4.1}$$

where ω is frequency and t is time. The resistance to the motion of the ratchet head is represented approximately in Fig. 4.4. This is a force which uniformly resists the motion of the head during each half-cycle of oscillation. For design purposes the maximum force is used to size the device, since any lower value of this resistance simply means that a smaller driving signal is needed at the input. The dynamics of the system thus described is approximated by that of a friction damped oscillator where the frictional force obeys the coulomb law. The condition for sustained oscillation is (see Ref. 7):

$$e > 4F/(\pi K) \tag{4.2}$$

where K is the spring rate and F is the resistance. The design considerations for the selection of the spring rate K are as follows:

(1) The required frequency for resonant oscillation of the ratchet head is directly proportional to the square root of K and inversely proportional to the square root of the mass of the ratchet head. This frequency is determined by the required time constant for the deflection of the servoflaps.

(2) As seen in the above inequality, the higher the permissible value of K the less displacement input is required from the piezoelectric stack for a fixed value of the resistance F. Since piezoelectric ceramics output very small displacements, it is desirable to make K as

20

high as possible.

Feasibility Assessment: Flight test data on the Kaman SH-2F helicopter was obtained from Kaman Aerospace Corporation. This data provided measured values of the control loads on the chordwise rod which is used to deflect the servoflaps on the H-2 composite main rotor blade. Using this information as nominal loads which must be overcome by the proposed device, an analysis of the design feasibility of the concept was performed. This analysis showed that it is possible to design a piezoelectrically actuated system to control the servo-flap on an SH-2F class helicopter from hover to full forward speed of 144 knots. The control system on the SH-2F helicopter consists of a servoflap which is deflected to produce aerodynamic moments which deform the torsionally soft main rotor blade. The deflection of this servoflap is achieved via an arrangement of linkages which ultimately displace a chordwise rod which produces a moment about the hinge axis of the servoflap via an offset horn. Flight test data show that the loads measured from this chordwise rod are no more than 90 lbs steady compressive + or - 42 lbs vibratory (1/rev).

Consider the piezoelectric stack shown in Fig. 4.3. N is the number of plates, each of thickness t, resulting in an overall length of L = N.t. The electrical connections to the electrodes of the plates are such that a voltage V is applied to all the plates simultaneously, resulting in a field strength of (V/t) volts/meter across each plate. The thickness strain produced in each plate is ε = (V/t).d_{33}, where d_{33} is the Piezoelectric Constant = Strain/Field at constant stress. Since the deformation of all the plates add up to the overall deformation of the stack, ε also equals e/L. Hence:

$$e = (V/t).d_{33}.L \tag{4.3}$$

The requirement for sustained oscillation of the resonant system is that e > 4F/(πK), where F is the resisting force and K is the spring constant of the model Before plugging this condition into Eq. 4.3, the spring constant can be replaced by K = m.ω^2 where m is the effective mass of the driving head and ω is the operating frequency (resonant for the combination of m and K). The limiting value for the resisting force, beyond which steady oscillations will not be sustained is therefore given by:

$$F < (\pi/4).(V/t).d_{33}.L.m.\omega^2 \tag{4.4}$$

The following are the pertinent properties of PZT-5H ceramic (Ref.1) -
Piezoelectric Constant, i.e Strain/Field at constant stress

$$d_{33} = 593 \times 10^{-12} \text{ meters/volt}$$

$$\text{A/C depoling field, } (V/t)_{max.} < 4 \times 10^5 \text{ volts/meter}$$

$$\text{Frequency Constant (thin plate), } N_{3t} = f_R \times t$$
$$= 2000 \text{ cycle } \times \text{ meters/second}$$

The frequency constant for a thin plate of thickness t helps to determine an operating frequency $f < f_R$ which is below the resonant frequency of the plate itself. On the other hand a high operating frequency is desired for two reasons - (1) to keep the mass of the driving head low and (2) to have a bandwidth which is many times the 1/rev of the helicopter. For this reason the plates should be as thin as the A/C depoling field intensity will permit.

For a design using PZT-5H, with $(V/t) = 10^5$ volts/meter, $\omega = 10^4$ radians/sec., $L = 0.25$ meters, Eq. 2 gives:

$$F < 1164.m \text{ Newtons} = 262.m \text{ lb. (approx.)} \tag{4.5}$$

with m in kilograms. Thus for an effective mass of the drive head of the order of 1 kilogram (2.2 lb.), a system which will control the servoflap of an SH-2F can be designed quite readily. Note that the mass of the system can be reduced further if a higher operating frequency is used.

4.3 Power Requirements

The power consumption of the proposed system is composed of contributions from the power required to produce the mechanical power for the intended actuation, and the power require to compensate for dissipative losses both within the elements of the piezoelectric stack and in the mechanical assembly attached to the stack. Data for the estimation of the power due to internal and mechanical losses, are obtainable only from an experimental study. With the understanding that the power calculated from analysis only is only a lower bound on the actual power consumed, the following analysis will not include the effects of internal dissipation in the piezoelectric stack and the mechanical losses in the assembly. Moreover, in order to relate the analysis to a physically realizable system, a design of the piezoelectric actuator which can conceivably replace the servoflap actuation system in the Kaman SH-2F helicopter will be used for the analysis.

Mechanical Power:

The sketch shown in Fig. 4.4 illustrates a possible arrangement for generating displacements of the chordwise rod on the Kaman SH-2F helicopter. The variation of the area of the plates obeys a general power law so as to simplify the terms in the differential equations which depend on the area variations:

$$A(x) = A_1(A_2/A_1)^{x/L} \qquad (4.6)$$

where A_1 is the area at the wide end, and A_2 is the area at the narrow end. L is the overall height of the stack, and x is the coordinate dimension along the axis of the stack. A conceivable method for transforming the oscillatory motion of the resonant output into the linear displacements needed by the chordwise rod is to feed control signals to a separate pair of piezoelectric plates which intemittently couples the oscillation of the actuator end with the chordwise rod in such a way that the chordwise rod moves only in the direction desired. In other words, if it is desired to move the rod in a given direction, the couplers are energized to connect (by generating normal forces which cause enough friction to prevent the relative sliding between the actuator and the chordwise rod assembly) the driver to the chordwise rod only when the driver is moving in the desired direction. The graph of the displacement of the chordwise rod with time looks somewhat like Fig. 4.6. During each half cycle of the oscillations of the driver, the chordwise rod is advanced by twice the amplitude of the driver's oscillations. In the other half cycle, its displacement is considered zero (this can actually be accomplished by yet another pair of stacks which holds the rod fixed to the blade to prevent its traction in the opposite direction). If the amplitude of oscillation of the driver is a_d, then the average velocity of the rod translation over each cycle of the driver's oscillation is:

$$U_r = \omega.a_d/\pi \qquad (4.7)$$

Eq. 4.7 also facilitates an estimation of the amplitude of the driver which is required for imposing a given speed on the chordwise rod. For example, using the measured data on the SH-2F; the peak amplitude of the 1-per-rev deflection of the servoflap is 7.71 degrees at 298 rpm. This corresponds to a peak angular velocity of 4.2 radians/second. With flap-horn offset of 2.5 inches (or 6.35×10^{-2} meters), the peak translational velocity of the chordwise rod $(U_r)_{peak} = 26.67 \times 10^{-2}$ m/s. If the operating frequency of the resonant system is 10^4 rad./sec., then the required peak amplitude of the drive head $(a_d)_{peak} = 83.78 \times 10^{-6}$ meters.

In the configuration being considered, the drive head experiences

resistance only during every half cycle, when it is fully coupled to the chordwise rod (see Fig. 4.6). The peak work per cycle $(W_c)_{peak}$ = $2.F_{peak}.(a_d)_{peak}$. Peak power output, averaged over each cycle of oscillation of the driver:

$$(P_c)_{peak} = (W_c)_{peak}.\omega/(2.\pi) \tag{4.8}$$

Using a value of 150 lb. (667.2 Newtons) as the peak force (slightly higher than the forces measured on the SH-2F), the peak mechanical power output of the piezoelectric actuator assembly is about 178 watts. This number should be considered a conservative estimate, since the calculations assume that the peak forces are being applied at peak velocities. This is not necessarily so, since a phase shift always exists between the applied forces and the velocities. However, since mechanical losses and internal piezoelectric losses have not been taken into account, it is probably safer to consider a 200 watt system for controlling the servoflap of each blade on a helicopter comparable to the SH-2F.

Electrical Power:

The electrical power required to drive the piezoelectric stack is related to the mechanical power output via the square of the coupling constant k_{33}:

$$P_{electrical} = P_{mechanical}/k_{33}^2 \tag{4.9}$$

For the piezoelectric material PZT-5H, $k_{33} = 0.752$. In order to output a mechanical power of 200 watts, the electrical power required is 354 watts.

The voltage and current characteristics required from the power supply is dependent on such design factors as: plate thickness t, total capacitive area of the stack A_c, and the number of plates in the stack. The thickness of the stack governs the required voltage supply in order to achieve the desired electrical field strength. The total capacitive area governs the value of the capacitance C_E, which in turn determines the turns ratio of the equivalent transformer circuit, as was show in chapter 3.

Chapter 5 - Practical Design Issues

5.1 Actuator System Components

The key to the practical usage of the piezoelectric actuator technology for the control of helicopter rotorblade aerodynamics is in the development of components for the excitation and control of the piezoelectric stacks and the drive-head. The schematic of Fig. 5.1 shows the major components needed for the piezoelectric actuator system. The nomenclature of piezoelectric stack and drive-head are consistent with those of Fig. 4.5. The system shown in Fig. 5.1 essentially replaces all the mechanical components associated with the deflection of servo-flaps on a helicopter such as the Kaman SH-2, including the swash-plate and control rods. The signal to deflect the servoflap is fed to a *Waveform Generator* as well as the actuator *Controller* after being compared to the actual deflection of the servoflap by a *Feedback Sensor*. The signal from the Waveform Generator is amplified into a low voltage-high current signal by the *Amplifier* which derives its electrical power from the *Power Supply*. The Power Supply, Amplifier, Waveform Generator and the Deflect Flap Signal are situated in the non-rotating frame. Both signals from the Deflect Flap Signal and the Amplifier pass through *Slip Rings* into the rotating frame.

In the rotating frame, the *Transformer* converts the low voltage signals into high voltage signals. The *Controller* performs three basic tasks: (1) It controls the phases of the signals which are fed into the *Piezoelectric Stack* and the *Drive Head Control Stack* in such a way as to maintain the direction of displacement of the push-rod which deflects the servoflap. Note that the displacement of the push-rod occurs incrementally in half-cycles of the piezoelectric stack vibrations (see Fig. 4.6); (2) It schedules the activation and deactivation of the piezoelectric stack, based on the relative state of the servoflap and the demand signal for servoflap deflection; (3) It modulates the amplitude of the signals which are fed into the piezoelectric stack in such a way as to maintain the required response of the drive-head. The research and development of these components for a bench-top model of the piezoelectric actuator system will be the subject of the Phase II SBIR proposal.

5.2 Operating Frequency

The operating principle of the actuator system relies on the elastic coupling between the drive-head and the piezoelectric stack via a linear spring. The idea is to magnify the displacement of the drive-head using the resonance of the spring-mass assembly. The displacement of the push-rod which deflects the servo-flap (see Fig. 4.5) occurs by clutching the drive-head to the push-rod every half-cycle of the oscillations in which the direction of motion of the drive head is in the appropriate direction. The resonance frequency is determined by the relationship between the mass of the drive-head and the stiffness of the coupling. As indicated in the previous chapter, it is desirable to place this frequency at several multiples of the bandwidth of the servo-flap deflection. The logic of this is simply that the precision of positioning the servoflap is enhanced if the incremental motions of the push-rod are much smaller than the overall displacement required to achieve maximum deflection of the servo-flap. The resonant frequency does not constitute a restriction on the application of the actuator system.

An alternative way of understanding the role of this frequency is to compare it to the role of the clock frequency in a digital to analog converter. The higher the clock frequency in relation to the highest frequency component of the analog signal, the better the resolution of conversion from the digital signals to the analog signals. Here the incremental motions of the drive-head at each half cycle is analogous to the train of digital signals which add up to the analog signal, whereas the motion of the push-rod and hence the deflection of the servoflap corresponds to the analog signal. As a matter of fact, this aspect of the actuator system indicates that it should be feasible to implement a fully digital controller for the system.

5.3 Aerodynamic Loading

The overall forces acting on the servoflap which include the aerodynamic, inertial and elastic forces are perceived by the drive-head as resistance forces which tend to impede its displacement each half-cycle that it is clutched to the push-rod. In the feasibility analysis, measured values of the extreme case from the Kaman-SH-2F helicopter were used to assess whether or not the vibrations of the drive-head will be sustained if these resistance forces were treated as coulomb dampers - using the maximum resistance values as constant over each half-cycle. The conclusion was that the vibrations of the drive-head can be sustained. It is important to note that the servoflap is not vibrating along with the drive-head at the same frequency, hence

26

the aerodynamic forces are not seen directly by the drive-head as damping forces. The approach of using representative values from measured data seems to be more realistic than any elaborate theoretical calculation of the aerodynamic forces.

5.4 Assessment of Centrifugal Effects

The piezoelectric coefficients that were used in the preceding analysis presume the absence of transverse stresses on the active elements. This condition will be violated somewhat by centrifugal loading due to the rotation of the helicopter blades. This effect in of itself is not expected to adversely impact the feasibility of the actuator. Other concerns with regard to centrifugal effects have to do with the structural strength of the system. The active elements, being basically ceramics are expected to have sufficient structural strength to withstand the centrifugal loading. The design which is envisaged as feasible will integrate the piezoelectric stacks into the profile of the rotorblade itself. It is conceivable that the ultimate version of the actuator will include load bearing elements. It is too early in the development to actually address the precise way in which the actuator elements will be loaded. These issues are expected to be resolved in the advanced developmental stages of the actuator system.

Chapter 6 - Concluding Remarks

Actuator Design: The studies which have been performed during the course of this research have yielded significant insights into the methods for designing piezoelectric actuators for the control of servoflaps on helicopter rotorblades. It was found that a stack of piezoelectric plates can be used to resonate a spring-mass substructure, thereby producing sufficient oscillatory motions which can be converted to linear or rotary motions for deflecting the servoflap. Using measured data from the Kaman SH-2F, it was shown that a system can be designed to drive the chordwise rod which deflects the servoflap of that helicopter. This design consists of a modification of the rotorblade to incorporate plates of piezoelectric ceramic PZT-5H. The electrical power required to produce the same forces and velocities measured on the Kaman SH-2F was found to be of the order of a few hundred watts. Alternative designs of the actuator could involve a complete redesign of the rotorblade. Such redesigns were not considered in this study. Also not considered were other ways of mechanizing the airfoil besides using a servoflap. The insights developed as a result of this research lead to a conlusion that substantial mechanization of helicopter rotorblades are feasible without severe weight penalties. It is in fact feasible to integrate the piezoceramics into the basic structural design of the blade.

SBIR Phase II Effort: Before the proposed concepts can be implemented on a rotorblade, further research is needed to obtain experimental data on the performance characteristics of the resonant piezoelectric driver. As a logical step, a bench-top demonstrator should be designed, fabricated and tested. Subsequent to this, a wind tunnel model should be designed, fabricated and tested. The issues that need to be resolved in these research efforts pertain to the structural integrity of the device under the dynamic environment of a rotorblade. The payoffs of a successful development of this technology are very significant. Substantial weight reductions in helicopter rotor system are possible because of the elimination of the assemblies that are ordinarily needed for transmitting control forces from the stationary frame to the rotational frame. Other payoffs include the implementation of controllers for alleviating rotor vibrations (e.g. Higher Harmonic Control, Adaptive Vibration Control etc) as well as controllers for delaying the onset of stall on the retreating blades, which has the potential benefit of expanding the performance envelope of the helicopter. It is the intention of AEDAR Corporation to compete for a Phase II award for continuing this research effort. A collaborative effort will be sought with Kaman Aerospace Corporation, which has substantial experience with the technology of servo-flap controlled helicopter blades.

APPENDIX

Properties of Some Commercially Available Piezoelectric Ceramics

(Ref. 1)

TABLE I

Typical Symbols Employed in Describing Properties of Piezoelectric Materials

Strictly speaking, these symbols are used to identify properties of MATERIALS only, and should not be used to describe characteristics of actual physical elements made of these materials. However, for convenience, some liberties have been taken in the explanations—electric boundary conditions are identified by indicating locations and connections of electrodes.

S_{11}^{D}

D — Indicates that compliance is measured with electrode circuit open

11 — Indicates that stress or strain is in 1 direction

— Indicates that strain or stress is in 1 direction

— Compliance $= \dfrac{\text{strain}}{\text{stress}}$

(All stresses, other than the stress involved in one subscript, are constant)

S_{36}^{E}

E — Indicates that compliance is measured with electrodes connected together

36 — Indicates that stress or strain is in shear form around 3 axis

— Indicates that strain or stress is in 3 direction

— Compliance $= \dfrac{\text{strain}}{\text{stress}}$

(All stresses, other than the stress involved in one subscript, are constant)

K_{1}^{T}

T — Indicates that all stresses on material are constant—for example: zero external forces.

1 — Indicates that electrodes are perpendicular to 1 axis

— relative dielectric constant $= \dfrac{\epsilon_{1}^{T}}{\epsilon^{o}}$

K_{3}^{S}

S — Indicates that all strains in the material are constant—for example: material completely blocked preventing deformation in any direction

3 — Indicates that electrodes are perpendicular to 3 axis

— relative dielectric constant $= \dfrac{\epsilon_{3}^{S}}{\epsilon^{o}}$

---

k_{15}

— Indicates that stress or strain is in shear form around 2 axis

— Indicates that electrodes are perpendicular to 1 axis

— Electromechanical coupling

k_{p}

— This subscript used only for ceramics. Indicates electrodes perpendicular to 3 axis, and stress or strain equal in all directions perpendicular to 3 axis

— Electromechanical coupling

---

d_{33}

— Indicates that the piezoelectrically induced strain, or the applied stress, is in 3 direction

— Indicates that electrodes are perpendicular to 3 axis

$\dfrac{\text{strain}}{\text{applied field}} = \dfrac{\text{short circuit charge/electrode area}}{\text{applied stress}}$

(All stresses, other than the stress involved in second subscript, are constant)

d_{h}

— Indicates that stress is applied equally in 1, 2, and 3 directions (hydrostatic stress); and that electrodes are perpendicular to 3 axis for ceramics or 2 axis for Lithium sulfate.

$\dfrac{\text{short circuit charge/electrode area}}{\text{applied stress}}$

---

g_{31}

— Indicates that applied stress, or piezoelectrically induced strain is in 1 direction

— Indicates that electrodes are perpendicular to 3 axis

$\dfrac{\text{field}}{\text{applied stress}} = \dfrac{\text{strain}}{\text{applied charge/electrode area}}$

(All stresses, other than the stress involved in second subscript, are constant)

g_{15}

— Indicates that applied stress, or piezoelectrically induced strain is in shear form around 2 axis

— Indicates that electrodes are perpendicular to 1 axis

$\dfrac{\text{field}}{\text{applied stress}} = \dfrac{\text{strain}}{\text{applied charge/electrode area}}$

(All stresses, other than the stress involved in second subscript, are constant)

33

TABLE II
Units and Description of Symbols

ϵ_O = dielectric constant of free space = 8.85×10^{-12} farads/meter.

ϵ^T/ϵ_O = relative dielectric constant, free.

ϵ^S/ϵ_O = relative dielectric constant, clamped.

$\tan \delta = \dfrac{1}{Q_E}$ = dissipation factor at 1 kcps, low electric field.

k_p = planar coupling factor.

k_{31} = transverse or lateral coupling factor.

k_{33} = longitudinal coupling factor.

k_{15} = shear coupling factor.

k_t = thickness coupling factor (laterally clamped).

d = piezoelectric constant, strain/field at constant stress or charge density /stress at constant electric field, 10^{-12} meters/volt.

g = piezoelectric constant, electric field/stress at constant charge or strain/charge density at constant stress, 10^{-3} volt meters/newton.

s^E = elastic compliance at constant electric field, 10^{-12} meter²/newton.

s^D = elastic compliance at constant charge density, 10^{-12} meter²/newton.

Q_M = mechanical Q. This is dependent upon configuration, and is given here for a thin disc.

N_1 = frequency constant of a thin bar, $f_R . \varrho$, cycle meters/second.

N_{3a} = frequency constant of a long slender bar electroded on ends, $f_a . \varrho$, cycle meters/second.

N_{3t} = frequency constant of a thin plate, $f_R . t$, cycle meters/seconds. ✛

v_3^D = velocity of a compressional wave parallel to polar axis $\{c_{33}^D = (v_3^D)^2 \rho\}$, meters/second.

v_4^D = velocity of a shear wave perpendicular to polar axis with wave polarization parallel to polar axis $\{c_{44}^D = (v_4^D)^2 \rho\}$, meters/second.

v_4^E = velocity of a shear wave parallel to polar axis, $\{c_{44}^E = (v_4^E)^2 \rho\}$, meters/ second.

ρ = density, 10^3 kg/m³.

ϕ = temperature, °C.

P = polarization, 10^{-6} coulomb/cm² (10^{-2} coulomb/m²).

α = thermal expansion, 10^{-6}/°C.

34

TABLE III
Piezoelectric Ceramics—Typical Room Temperature Data (Low Signal)

		Ceramic B	PZT-4	PZT-5A	PZT-5H	Preliminary data PZT-8
At one kcps*	$\epsilon_{33}^{T}/\epsilon_o$	1200	1300	1700	3400	1000
	$\epsilon_{33}^{S}/\epsilon_o$	910	635	830	1470	600
	$\epsilon_{11}^{T}/\epsilon_o$	1300	1475	1730	3130	—
	$\epsilon_{11}^{S}/\epsilon_o$	1000	730	916	1700	—
	$\tan \delta$	0.006	0.004	0.02	0.02	0.004
	k_p	−.33	−.58	−.60	−.65	−.50
	k_{31}	−.194	−.334	−.344	−.388	−.295
	k_{33}	.48	.70	.705	.752	.62
	k_{15}	.48	.71	.685	.675	—
	k_t	.384	.513	.486	.505	—
	k_{i3}	.491	.715	.715	.754	.63
	d_{31}	−58	−123	−171	−274	−93
	d_{33}	149	289	374	593	218
	d_{15}	242	496	584	741	—
	d_h	33	43	32	45	.32
	g_{31}	−5.5	−11.1	−11.4	−9.11	−10.5
	g_{33}	14.1	26.1	24.8	19.7	24.5
	g_{15}	21.0	39.4	38.2	26.8	—
	s_{11}^{E}	8.6	12.3	16.4	16.5	11.1
	s_{33}^{E}	9.1	15.5	18.8	20.7	13.9
	s_{44}^{E}	22.2	39.0	47.5	43.5	—
	s_{12}^{E}	−2.6	−4.05	−5.74	−4.78	−3.7
	s_{13}^{E}	−2.7	−5.31	−7.22	−8.45	−4.8
	s_{11}^{D}	8.3	10.9	14.4	14.05	10.1
	s_{33}^{D}	7.0	7.90	9.46	8.99	8.5
	s_{44}^{D}	17.1	19.3	25.2	23.7	—
	s_{12}^{D}	−2.9	−5.42	−7.71	−7.27	−4.5
	s_{13}^{D}	−1.9	−2.10	−2.98	−3.05	−2.5
	Q_M	400	500	75	65	1000
	N_1	2290	1650	1400	1420	1700
	N_{3t}	2740	2000	1890	2000	—
	N_{3a}	2530	2060	1845	1930	2000
	ρ	5.55	7.5	7.75	7.5	7.6
	Curie Point	115°C	328°C	365°C	193°C	300°C

*For PZT-5A the dielectric constants decrease about 2.4%/decade of frequency to at least 20 mcps and increase 2.4%/decade of frequency below 1 kcps to at least 1 cps.
For PZT-4 the dielectric constants decrease about 1.0%/decade of frequency to at least 1 mcps and increases 1.0%/decade of frequency below 1 kcps to at least 1 cps.

TABLE IV

Temperature and Time Stability

	Ceramic B	PZT-4	PZT-5A	PZT-5H	Preliminary data PZT-8
Change in k_p/time decade	−1.8%	−2.3%	−0.2%	−0.3$_5$%	−2
Change in ϵ_{33}^T/time decade	−0.8%	−5.8%	−1%	−1.5%	−5
Change in N_1/time decade	+0.5%	+1.5%	+0.2%	+0.2$_5$%	+1
Volume resistivity in ohm meters					
25°C	$>10^{10}$	$>10^{10}$	$>10^{11}$	$>10^{11}$	$>10^{10}$
100°C	$10^{7.5}$	$10^{8.5}$	10^{11}	10^{11}	$>10^{8.0}$
200°C	10^5	$10^{6.5}$	10^{10}	10^{10}	
Time constant, seconds					
25°C	>100	>100	>2000	>2000	~100
100°C	~0.3	~5	~1800	>2000	~2
200°C	~0.002	~0.07	~250	~1000	

TABLE V

High Signal Properties

(In this Table units of electric field are kv/cm or 10^5 volts/m rms and stress in psi peak)

	Ceramic B	PZT-4	PZT-5A	PZT-5H
AC depoling field	3.5	>10	7	~4
AC field for tan δ = 0.04, 25°C a)	1.7	3.9	0.45	0.3
% increase of ϵ_{33}^T at above electric field.	—	17	11	5.3
AC field for tan δ = 0.04, 100°C.	1.0 at 75°C	3.3	0.45	0.2
Maximum rated static compressive stress (maintained) PARALLEL to polar axis. 25°C	2,000	12,000	3,000 or 5,000c)	1,500 or 2,000c)
100°C	1,000 at 75°C	6,000	3,000	1,000 or 1,500c)
% change of ϵ_{33}^T with stress increase to rated maximum compressive stress at 25°C b)	—	+25% approx.	−3% approx. d)	e) −4% approx.
% change of d33 with stress increase to rated maximum compressive stress at 25°C. b).	—	±15% approx.	−0% at 3,000 −13% at 5,000 approx.	−5% at 1,500 −7% at 2,000 approx.
Maximum rated compressive stress (cycled) PARALLEL to polar axis 25°C	2,000	12,000	3,000	2,500
100°C	1,000 at 75°C	6,000	3,000	2,000
Maximum rated static compressive stress (Maintained) PERPENDICULAR to polar axis 25°C	2,000	8,000	2,000	1,500
100°C	1,000 at 75°C	4,000	2,000	1,000
% change of ϵ_{33}^T with stress increase to rated maximum compressive stress at 25°C. b)	—	+10% approx.	—	—
% change of d31 with stress increase to rated maximum compressive stress at 25°C. b)	—	−10%f approx.	—	—
Maximum rated hydrostatic pressure	20,000	50,000	20,000	20,000
Compressive strength	>50,000	>75,000	>75,000	>75,000
Tensile strength, static	7,500	11,000	11,000	11,000
tensile strength, dynamic (peak) g)	3,000	3,500	4,000	4,000
Mechanical Q at ~0 psi	400	500	75	65
Mechanical Q at 1,000 psi (peak dynamic stress)	140 approx.	180 approx.	25 approx.	—
Mechanical Q at 2,000 psi (peak dynamic stress)	85 approx.	110 approx.	25 approx.	—
% increase in s_{11}^E at 1,000 psi	1.7 approx.	1.7 approx.	10.5 approx.	—
% increase in s_{11}^E at 2,000 psi	3.7 approx.	3.7 approx.	17 approx.	—
Polarization 25°C	8μ coul/cm²	30	38	33
Coercive Field 25°C	~5	h)	12	6.5

a) The value of tan δ at a given electric field is a function of time after poling or after any major disturbance such as exposure to an elevated temperature.

b) After appropriate stabilizing treatment. This consists of the temperature stabilization discussed previously plus a few minutes soak at the appropriate static stress. The temperature stabilization is, however, more important than the stress soak.

c) The higher figure applies to a receiver, the lower to a radiator. The recommended use of PZT-5A or PZT-5H is the former.

d) In range to 10,000 psi.

e) In range to 5,000 psi.

f) The lateral d-constant perpendicular to the stress and polar axis is up about 20%.

g) These figures are dependent upon configuration and perfection of fabrication. The static tensile strength figures were obtained from bending tests on thin "Bimorph" structures, while the dynamic tensile strength figures were obtained from measurements of high amplitude resonant vibration of rings. The latter tests are more sensitive to minor flaws.

h) Coercive field values for PZT-4 are not well defined, as values from hysteresis loops are time dependent and dependent on amplitude of peak electric field.

i) Coercive field is quasi static value; it is not rms.

37

TABLE VI
Thermal Effects

A. Pyroelectric effects, $(\partial P/\partial \theta)_T$ in 10^{-6} coul/cm^2 °C (10^{-2} coul/m^2°C)

Temperature, °C	Ceramic B[b] First Heating	PZT-4 First Heating	PZT-5A First Heating	PZT-5A Subsequent Heatings
−196	—	—	−0.02	−0.02
− 80	−0.025	−0.025	−0.03	−0.02
− 60	−0.025	−0.025	−0.03	−0.02
0	−0.022	−0.025	−0.04	−0.02
30	−0.022	−0.028	−0.06	−0.02
60	−0.022	−0.026	−0.07	−0.02
80	(a)	−0.025	−0.09	−0.02
100	(a)	(a)	−0.11	−0.02
200	0	(a)	−0.17	−0.04
300	0	(a)	−0.23	−0.09

a) Above about 80°C the pyroelectric effect is masked by anomalous dielectric charges.
b) Ceramic B has a very sharp peak in the pyroelectric constant at the orthorhombic-tetragonal phase transition near −30°C. The peak value is about 0.3 μcoul/cm^2°C.

B. Thermal Expansion Coefficient (α in 10^{-6}/°C)

	Poled PZT-5A First Heating α_1	α_3	Subsequent Heatings α_1	α_3	Poled PZT-4 First Heating α_1	α_3	Subsequent Heatings α_1	α_3
°C								
0	+1.5	+2	+1	+4	+1.5	+0.1	+3.8	+1.7
50	+1.5	+2	+1.4	+4	+4.5	−0.1	+3.8	+1.7
100	+6	−6	+2	+3	+5.8	−6	+3.8	−1
150	+6	−7	+2.7	+1	+6.4	−6	+3.8	−1.4
200	+5	−7	+3.3	−1.6	+5.4	−6.1	+3.4	−2.4
250	+4.2	−6	+3.9	−4.2				

	Virgin (Unpoled) PZT-5A α	PZT-4 α	°C	Ceramic B First Heating α_1	α_3
0	+2.5	+2.0	30	+7.5	+4.7
50	+2.1	+1.8	40	+7.5	+4.7
100	+2.0	+1.5	50	+7.5	+4.7
150	+1.8	+1.1	60	+7.5	+4.7
200	+1.5	+1.0	70	+7.5	+4.3
250	+1.0	+0.3	80	+7.5	+3.2
300	+0.7	0.0	90	+7.5	+1.8
350	−3.0	+6.2	100	+7.5	0
400	+5	+7.8		Above 120°C	
500	+8.2	+8.2		$\alpha = +9$	

As noted above, thermal expansion of PZT-4 and PZT-5A is extremely anisotropic only on first heating, and on first heating only above about 50°C. With Ceramic B thermal expansion is markedly anisotropic only above about 80°C even on first heating.

C. Heat Capacity.

PZT, ~420 joules/kg°C (138 joules/°C mole).
Ceramic B, ~500 joules/kg°C (117 joules/°C mole).

D. Thermal Conductivity.

PZT, ~1.8 watts/meter°C.
Ceramic B, ~2.5 watts/meter°C.

38
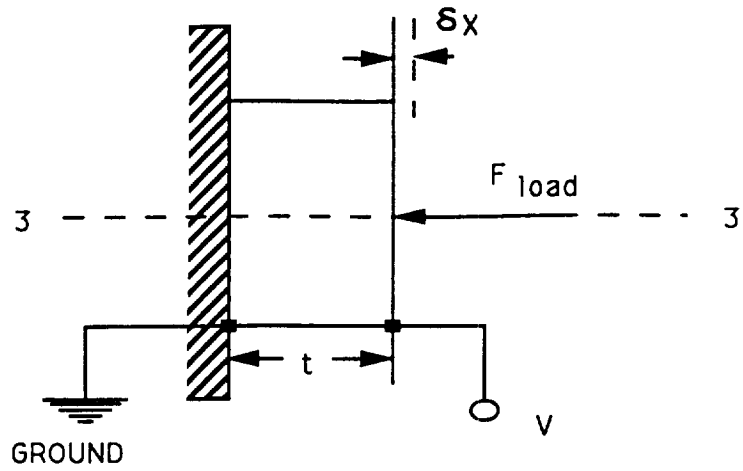
Figure 3.1. Single Element Thickness Expansion/Contraction
Piezoelectric Actuator
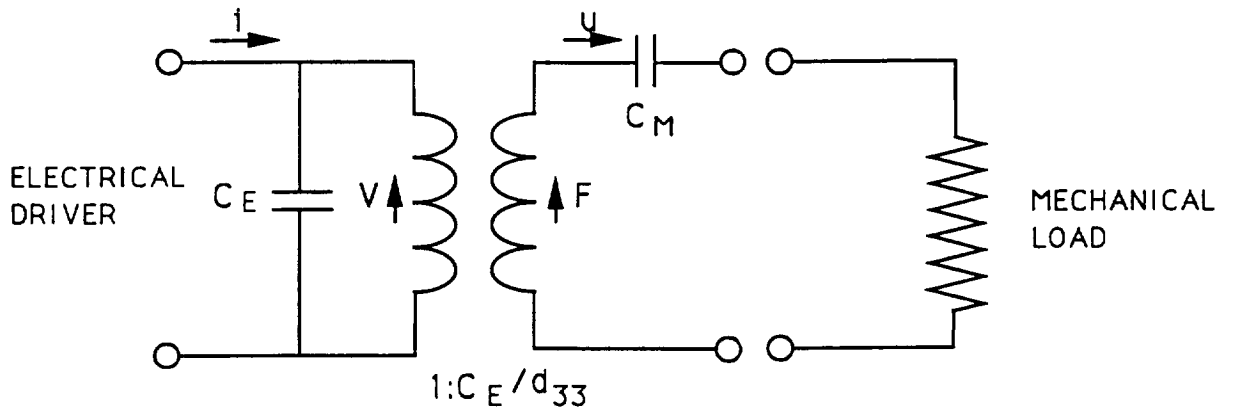
Figure 3.2 Electromechanical Model of Single Element Actuator

V

$A(L)$

F_{LOAD} — 3

3

t

$A(x)$

x

$=$ Gnd

L
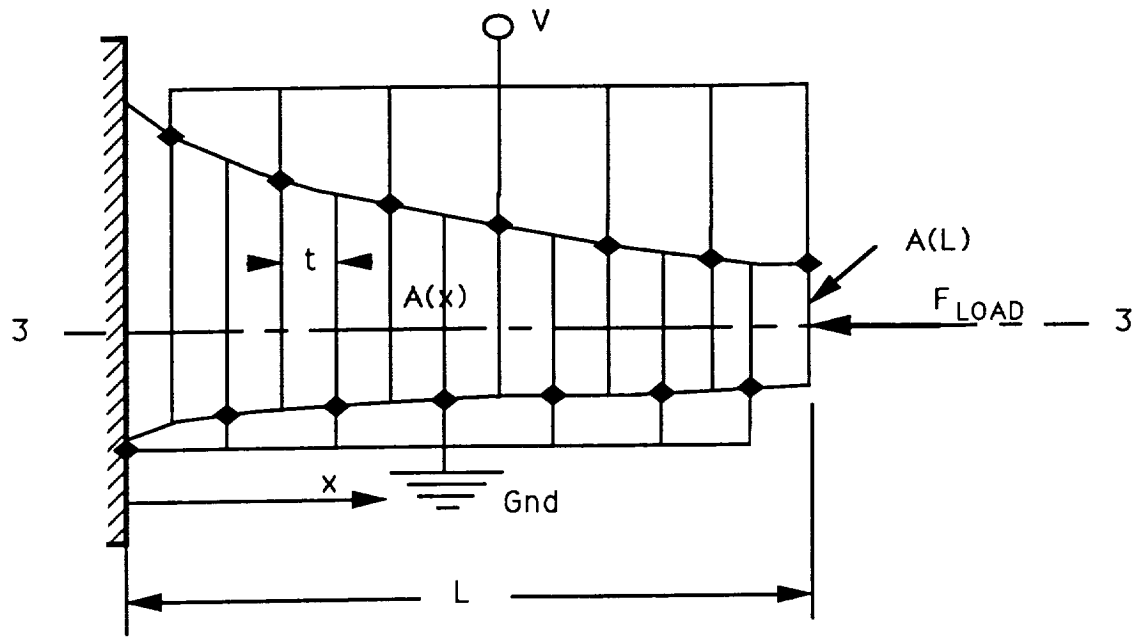
Figure 3.3 Schematic of Multi-element Piezoelectric Actuator

$\rho A(x) \dfrac{\partial^2 w}{\partial t^2} dx$

T

$T + \dfrac{\partial T}{\partial x} dx$

x

$A(x)$

$w + \dfrac{\partial w}{\partial x} dx$

$w(x,t)$
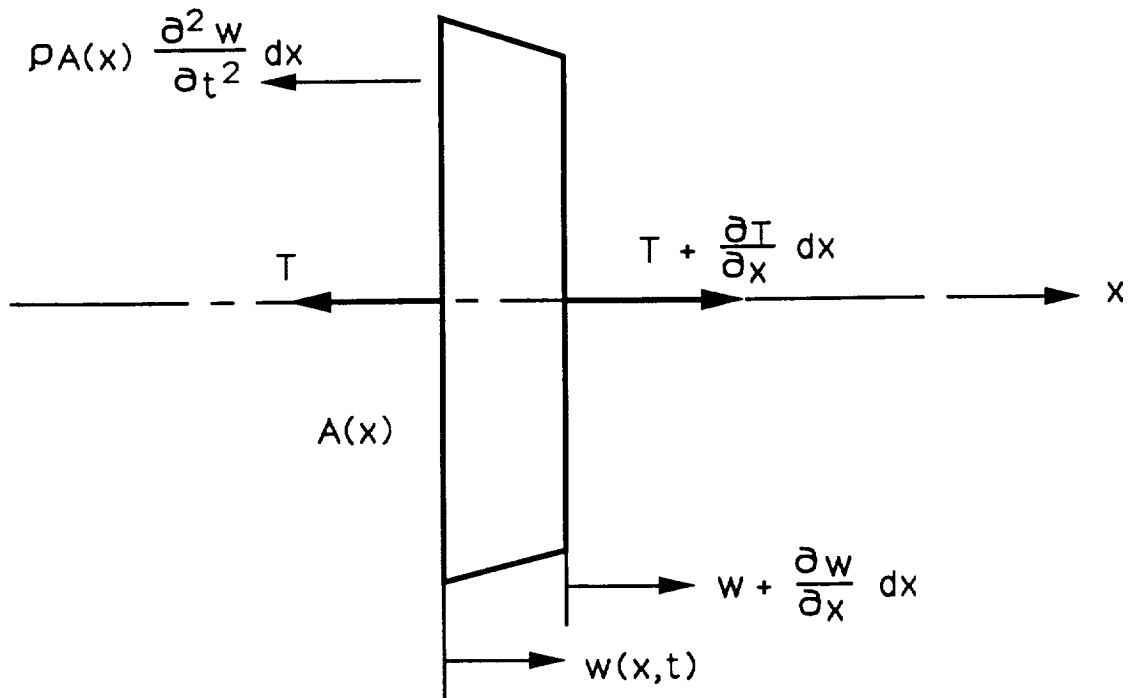
Figure 3.4 Equilibrium of an Infinitessimal Element of the Stack
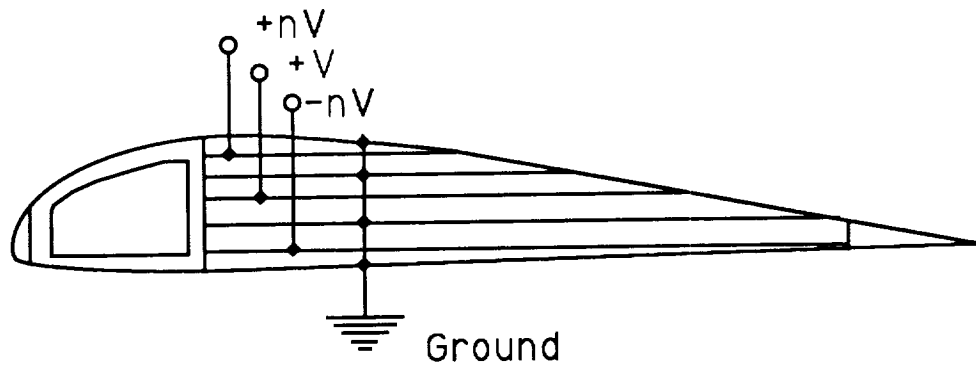
Figure 3.5 Schematic of Direct Bimorph Flap Concept
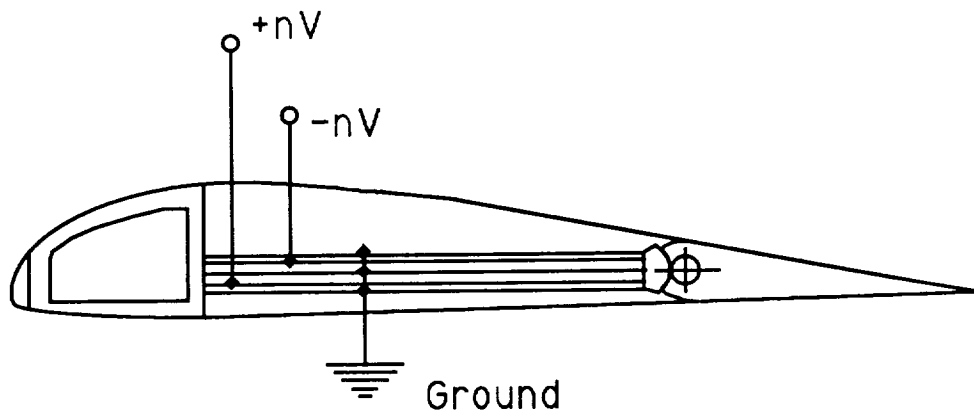
Figure 3.6 Schematic of the Bimorph Hinged Flap Concept
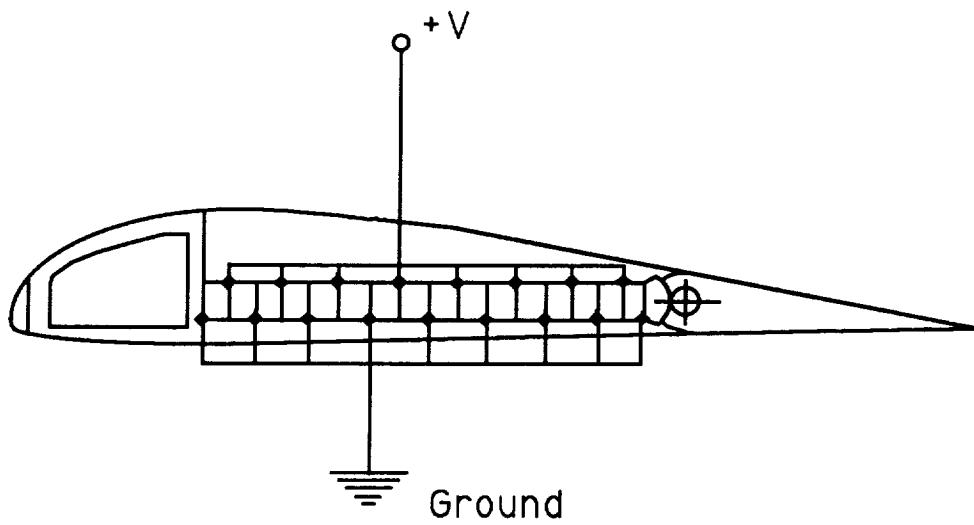
Figure 3.7 Schematic of the Transverse Shear Hinged Flap
Concept
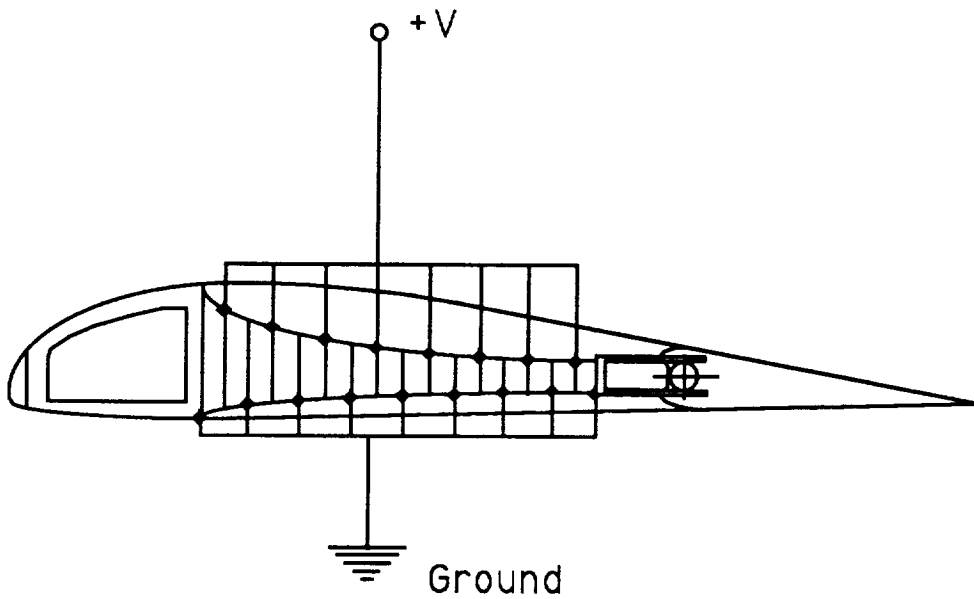
Figure 3.8 Schematic of the Thickness Expansion /
Contraction Hinged Flap Concept
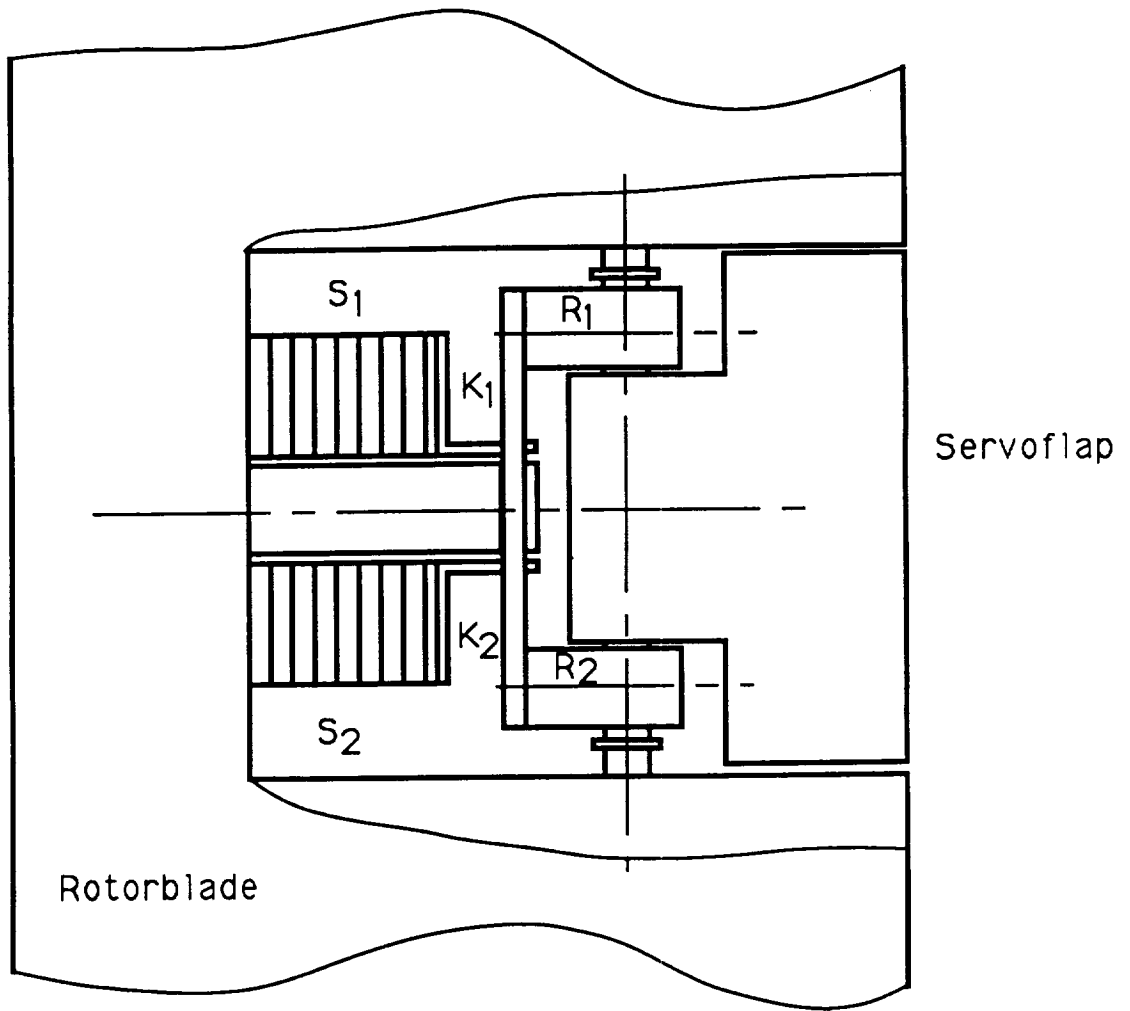
Figure 4.1. Schematic of Piezoelectric Actuator Assembly
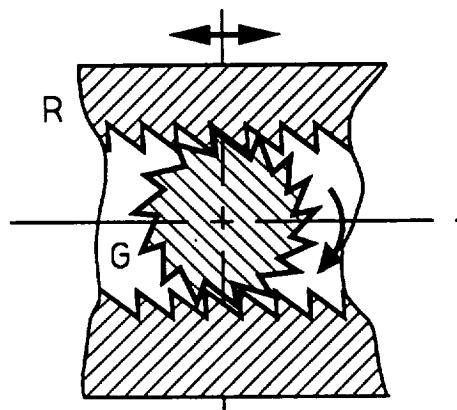
Figure 4.2. Illustration of Servoflap Rotation Drive-head

43
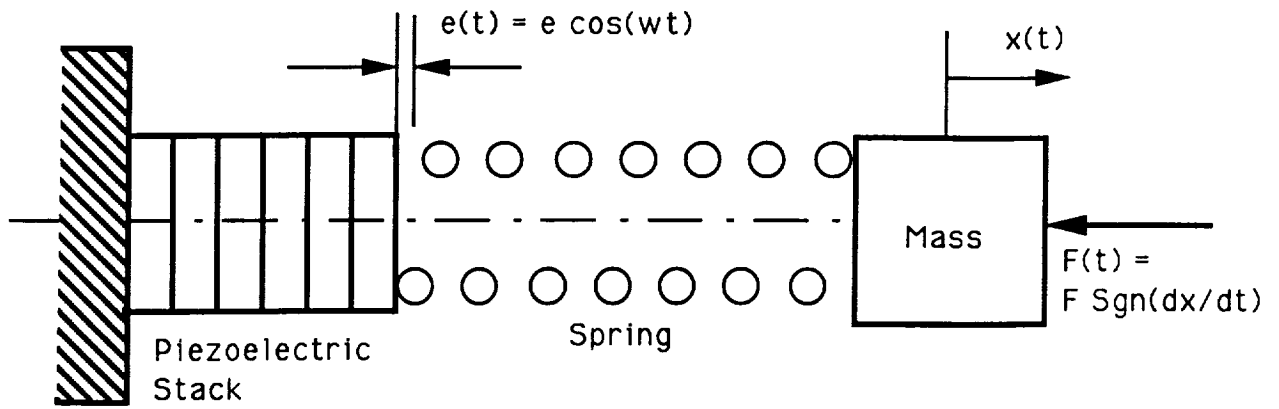
Figure 4.3. Dynamic Model of Actuator Mechanism
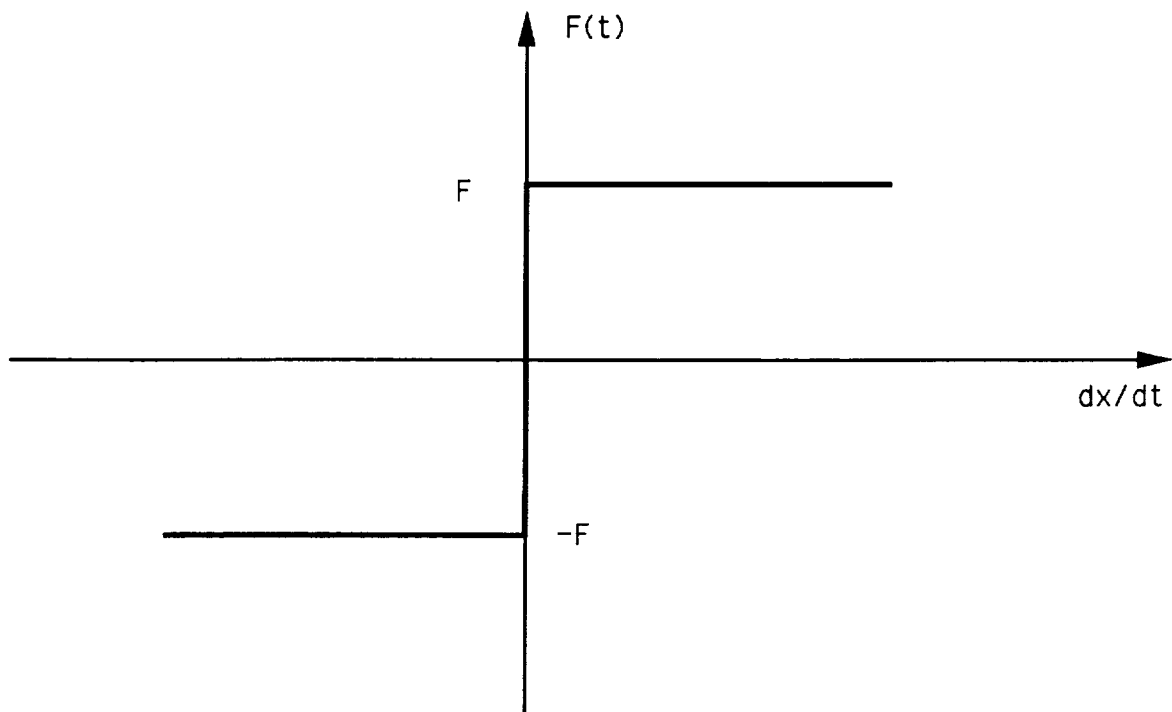
Figure 4.4. Resistance to Ratchet Head Motion
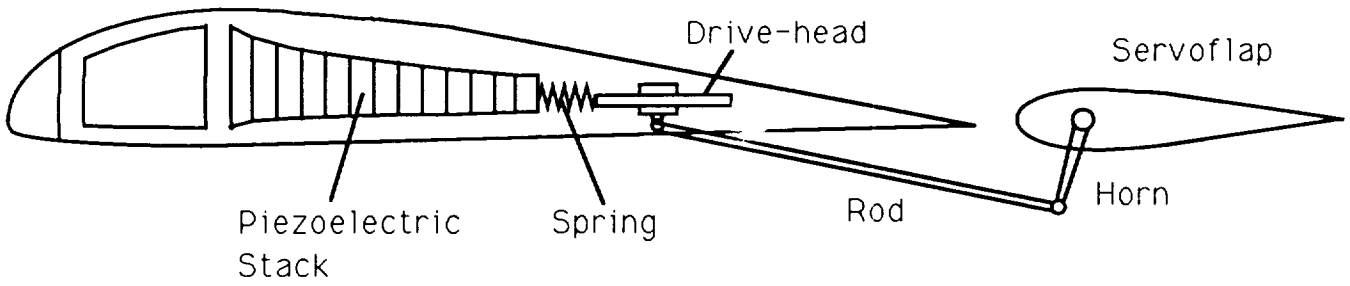
Figure 4.5. Possible Concept for Kaman SH-2F Servoflap Deflection
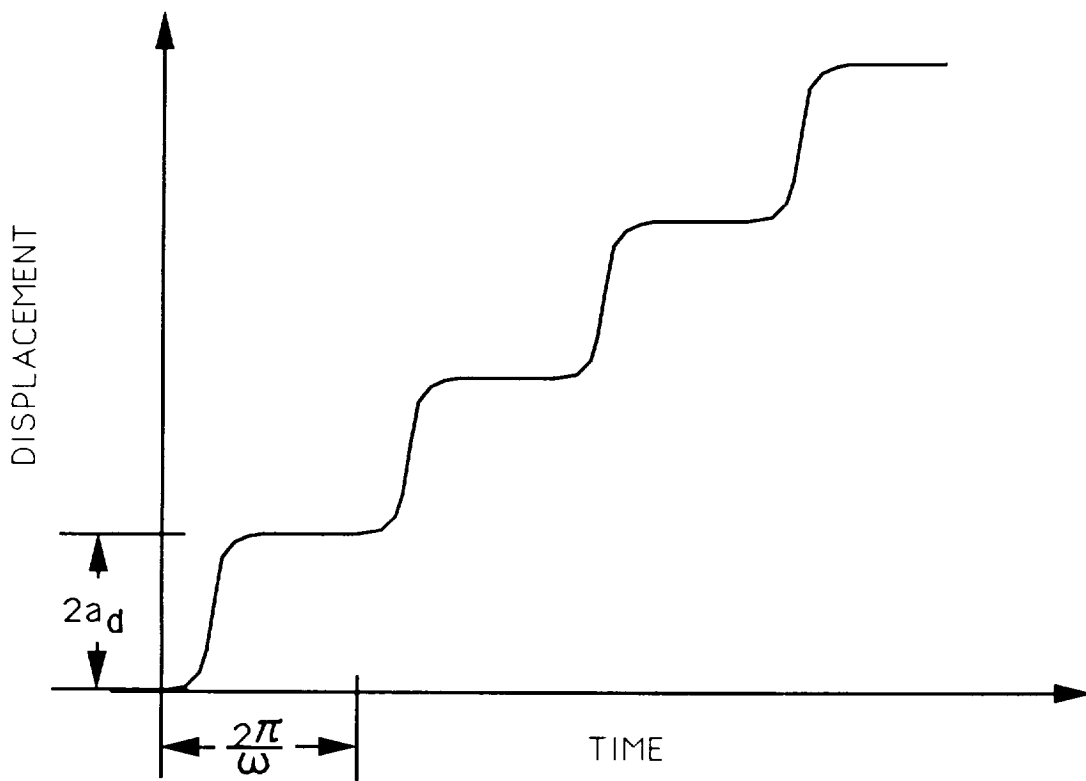
Figure 4.6. Graph of Chordwise Translation Induced by
Oscillatory Motions of the Drive-head

45
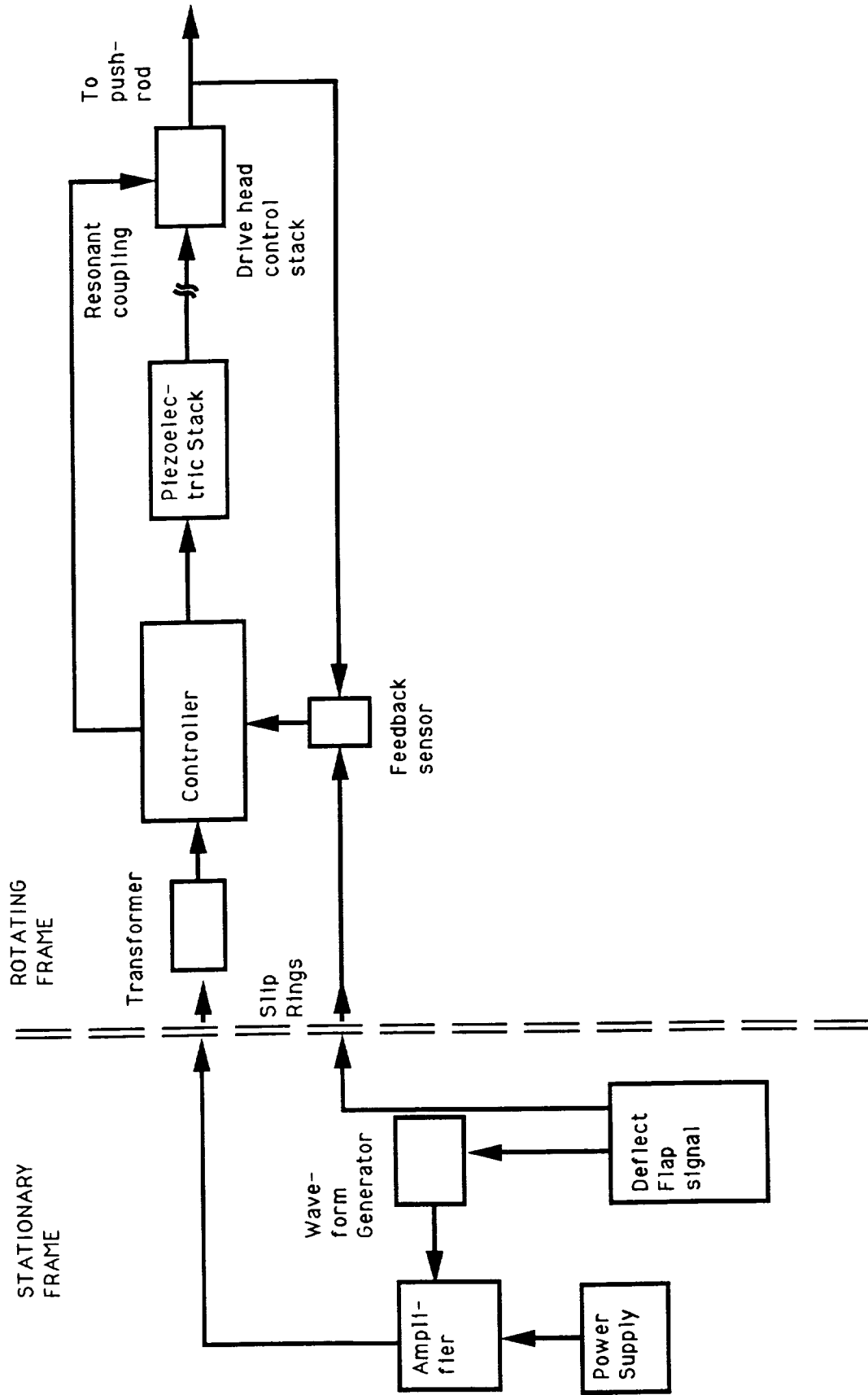
Figure 5.1. Schematic of Piezoelectric Actuator System

46

REFERENCES

1. Piezoelectric Technology – Data for Designers, Clevite Corporation, 1965.

2. Guide to Modern Piezoelectric Ceramics, Vernitron Corporation: Piezoelectric Division, Bedford, Ohio.

3. Keiko Koga; and Hiroji Ohigashi: Piezoelectricity and Related Properties of Vinylidene Fluoride and Trifluoroethylene Copolymers. J. Appl. Phys., vol. 59, no. 6, March 1986, pp. 2142-2150.

4. Butkovskiy, A. G. (L. W. Longdon, transl.): Structural Theory of Distributed Systems. Ellis Horwood Ltd., 1983.

5. Keener, James: Principles of Applied Mathematics: Transformation and Approximation. Addison-Wesley, 1988.

6. Fabunmi, J. A.: Analysis of Modes and Frequencies of Modified Structures Using Computer Algebra. Proceedings of International Conference on Noise and Vibration '89, Nanyang Technological Institute, Singapore, Aug. 1989.

7. Timoshenko, S.; Young, D. H.; and Weaver, W., Jr.: Vibration Problems in Engineering, Fourth ed. John Wiley & Sons, 1974.

16. Abstract

The results of a feasibility study of a method of controlling the aerodynamics of helicopter rotorblades using stacks of piezoelectric ceramic plates are presented. A resonant mechanism is proposed for the amplification of the displacements produced by the stack. This motion is then converted into linear displacement for the actuation of the servoflap of the blades. A design which emulates the actuation of the servoflap on the Kaman SH-2F is used to demonstrate the fact that such a system can be designed to produce the necessary forces and velocities needed to control the aerodynamics of the rotorblades of such a helicopter. Estimates of the electrical power requirements are also presented. An SBIR Phase II research program is suggested, whereby a bench-top prototype of the device can be built and tested. A collaborative effort between AEDAR Corporation and Kaman Aerospace Corporation is anticipated for future effort on this project.